ANTIOXIDANTS & REDOX SIGNALING
Volume 20, Number 2, 2014

DOI: 10.1089/ars.2012.5051

ORIGINAL RESEARCH COMMUNICATION

Protective Role of DNJ-27/ERdj5 in *Caenorhabditis elegans* Models of Human Neurodegenerative Diseases

Fernando Muñoz-Lobato,[1] María Jesús Rodríguez-Palero,[1,*] Francisco José Naranjo-Galindo,[1,2,*] Freya Shephard,[3] Christopher J. Gaffney,[3] Nathaniel J. Szewczyk,[3] Shusei Hamamichi,[4] Kim A. Caldwell,[4] Guy A. Caldwell,[4] Chris D. Link,[5] and Antonio Miranda-Vizuete[1,2]

Abstract

Aims: Cells have developed quality control systems for protection against proteotoxicity. Misfolded and aggregation-prone proteins, which are behind the initiation and progression of many neurodegenerative diseases (ND), are known to challenge the proteostasis network of the cells. We aimed to explore the role of DNJ-27/ERdj5, an endoplasmic reticulum (ER)-resident thioredoxin protein required as a disulfide reductase for the degradation of misfolded proteins, in well-established *Caenorhabditis elegans* models of Alzheimer, Parkinson and Huntington diseases. ***Results:*** We demonstrate that DNJ-27 is an ER luminal protein and that its expression is induced upon ER stress *via* IRE-1/XBP-1. When *dnj-27* expression is downregulated by RNA interference we find an increase in the aggregation and associated pathological phenotypes (paralysis and motility impairment) caused by human β-amyloid peptide (Aβ), α-synuclein (α-syn) and polyglutamine (polyQ) proteins. In turn, DNJ-27 overexpression ameliorates these deleterious phenotypes. Surprisingly, despite being an ER-resident protein, we show that *dnj-27* downregulation alters cytoplasmic protein homeostasis and causes mitochondrial fragmentation. We further demonstrate that DNJ-27 overexpression substantially protects against the mitochondrial fragmentation caused by human Aβ and α-syn peptides in these worm models. ***Innovation:*** We identify *C. elegans dnj-27* as a novel protective gene for the toxicity associated with the expression of human Aβ, α-syn and polyQ proteins, implying a protective role of ERdj5 in Alzheimer, Parkinson and Huntington diseases. ***Conclusion:*** Our data support a scenario where the levels of DNJ-27/ERdj5 in the ER impact cytoplasmic protein homeostasis and the integrity of the mitochondrial network which might underlie its protective effects in models of proteotoxicity associated to human ND. *Antioxid. Redox Signal.* 20, 217–235.

Introduction

From a medical point of view, the main challenge that our society will face in the near future is the management of the consequences of an aging population. Improvements of the living conditions in developed countries have gradually extended longevity, which, combined with decreasing birth rates, have resulted in a progressive increase in the percentage of elderly people in the population (28). As consequence of this greater life expectancy, our society is also witnessing an increase in aging-associated diseases, such as neurodegenerative diseases (ND).

The progression of many ND share common cellular and molecular mechanisms, including mitochondrial dysfunction,

[1]Centro Andaluz de Biología del Desarrollo (CABD-CSIC), Depto. de Fisiología, Anatomía y Biología Celular, Universidad Pablo de Olavide, Sevilla, Spain.
[2]Instituto de Biomedicina de Sevilla (IBIS), Hospital Universitario Virgen del Rocío/CSIC/Universidad de Sevilla, Sevilla, Spain.
[3]MRC/Arthritis Research UK Centre for Musculoskeletal Ageing Research, University of Nottingham, Royal Derby Hospital, Derby, United Kingdom.
[4]Department of Biological Sciences, The University of Alabama, Tuscaloosa, Alabama.
[5]Institute for Behavioral Genetics, University of Colorado, Boulder, Colorado.
*These two authors contributed equally to this work.

Innovation

Among the molecular mechanisms compromised in most neurodegenerative diseases (ND), those related to oxidative folding of proteins in the endoplasmic reticulum (ER) and to the degradation of misfolded proteins are of critical importance. Using C*aenorhabditis elegans* models that recapitulate pathological aspects of Alzheimer, Parkinson, and Huntington diseases, we have demonstrated that DNJ-27/ERdj5 plays a protective role in these models by modulating the aggregation levels of beta amyloid peptide, α-syn, and polyglutamine proteins. Moreover, our data suggest that DNJ-27/ERdj5 exerts this protective function by impacting on several subcellular compartments, such as ER, cytoplasm, and mitochondria. Thus, DNJ-27/ERdj5 arises as a novel therapeutic target to investigate the molecular basis of these ND.

oxidative stress, protein aggregation, and inclusion body formation (56, 74). Indeed, aberrant protein deposition has been consistently linked to etiologically diverse ND. Hence, it is widely accepted that beta amyloid peptide (Aβ) aggregation plays a central role in the pathogenesis of Alzheimer Disease (AD) (27), the most prevalent ND worldwide. Increasing evidence points to a causative role of the presynaptic protein alpha-synuclein (α-syn), a polypeptide with a propensity towards intracellular aggregation, in Parkinson Disease (PD) pathogenesis (66, 67). Likewise, CAG repeat-disorders, including Huntington Disease (HD), spinocerebellar ataxias, spinal, and bulbar muscular atrophy (50), are typically associated with polyglutamine expansions (polyQ) of greater than 40 residues that cause the specific disease-associated proteins to misfold and aggregate. However, whether aggregates are causal in ND progression remains controversial and a matter of intense debate as they have been linked to both toxicity (by being themselves the toxic species) and protection (by sequestering soluble oligomeric products regarded as the toxic species) (2, 47, 56, 77).

Caenorhabditis elegans has emerged as a very useful model organism for the study of ND due to its advantageous characteristics, including a well-defined cell lineage and anatomy, its transparency through its entire life cycle and its simple, well-established genetics. Several *C. elegans* transgenic models have been developed to study many pathological aspects of ND (7, 41, 58). In these models, the specific expression of aggregation-prone proteins, such as human Aβ, human α-syn, and polyQ fusion proteins in muscle and neuronal cells allows the study of the cellular and molecular processes disrupted by, and behind, the aggregation and the toxicity of these proteins (18, 29, 49).

Within cells, quality control mechanisms maintain protein homeostasis by ensuring both accurate protein folding and degradation of proteins that fail to adopt their native conformation (5). Disturbances of these cytoprotective processes can favor abnormal protein conformations with toxic effects. In this sense, among the different pathways that lead to, or protect from the pathological effects associated to the aggregation-prone proteins in ND, those involved in protein folding and degradation are among the most relevant (85). The endoplasmic reticulum (ER) is the subcellular organelle where proper protein folding is monitored and achieved. Proteins that pass ER quality control criteria continue to their final destinations through the secretory pathway, whereas non-native and unassembled subunits of multimeric proteins are degraded by the ER-associated degradation (ERAD) pathway (36). Alterations in ERAD or in the oxidative folding of proteins containing disulfide bonds have been unequivocally implicated in ND (13, 33, 78).

Thioredoxins (Trxs) are the major cellular protein disulfide reductases and, among other functions, they act as potent antioxidant defenses, have redox regulatory roles and display chaperone properties. An RNA interference (RNAi) screen designed to identify modulators of protein aggregation and toxicity among the members of the Trx family of redox proteins in *C. elegans* models of AD and PD (12, 25), identified *dnj-27* as the only gene that provided a protective role in the two models assayed. *C. elegans dnj-27* is the ortholog of mammalian ERdj5, an ER-resident protein involved in ERAD (11, 80). ERdj5 works as an ERAD enhancer in concert with ER-degradation enhancing mannosidase-like protein (EDEM), which selectively recognizes misfolded glycoproteins, and BiP, an ER-resident Hsp70 family chaperone (80). ERAD substrates frequently contain disulfide bonds that must be cleaved before their retrotranslocation and ERdj5 has been proposed to be involved in the reduction of the disulfide bonds of these misfolded proteins through its Trx domains, before their retrotranslocation (80).

We have found that *dnj-27* protects against the aggregation of Aβ, α-syn and polyQ containing proteins in *C. elegans*, as well as their associated pathological phenotypes. Importantly, this protective effect is also achieved to some extent when ERdj5, the human *dnj-27* ortholog, is expressed in worm ND models. Our findings point to *dnj-27/ERdj5* as a new potential target for protection from proteotoxicity. These results also emphasize how small disturbances in ER protein homeostasis can affect the aggregation and toxicity of pathological proteins leading to worsening of the phenotypes associated with ND.

Results

C. elegans dnj-27 is the ortholog of mammalian ERdj5

We previously identified the *C. elegans dnj-27* gene as the ortholog of human *ERdj5* by an *in silico* approach (11). *C. elegans* DNJ-27 and human ERdj5 proteins display a high amino acid sequence homology consisting of an N-terminal DnaJ/Hsp-40 domain followed by four Trx-like domains, with different CXXC redox active site motifs (Fig. 1A) (11). The three-dimensional structure of mouse ERdj5 has been recently solved (24) and revealed that the interface domain flanked by the first and second Trx domains (Trx-1 and Trx-2) also folds as two additional, but more divergent, Trx-like domains, that lack a redox-active CXXC motif (Trxb-1 and Trxb-2). These two newly identified Trx-like domains are also present in the DNJ-27 protein sequence (Fig. 1A).

We first aimed to determine the cells and tissues expressing *dnj-27* within the nematode. For this purpose, we generated transgenic animals harboring the transcriptional reporter *Pdnj-27::GFP*, which expresses green fluoresecent protein (GFP) under the control of the *dnj-27* promoter (2 kb upstream the ATG codon) (All strains used in this work are described in Supplementary Table S1; Supplementary Data are available online at www.liebertpub.com/ars). Similar to mammalian ERdj5 (11), DNJ-27 also displays a ubiquitous expression

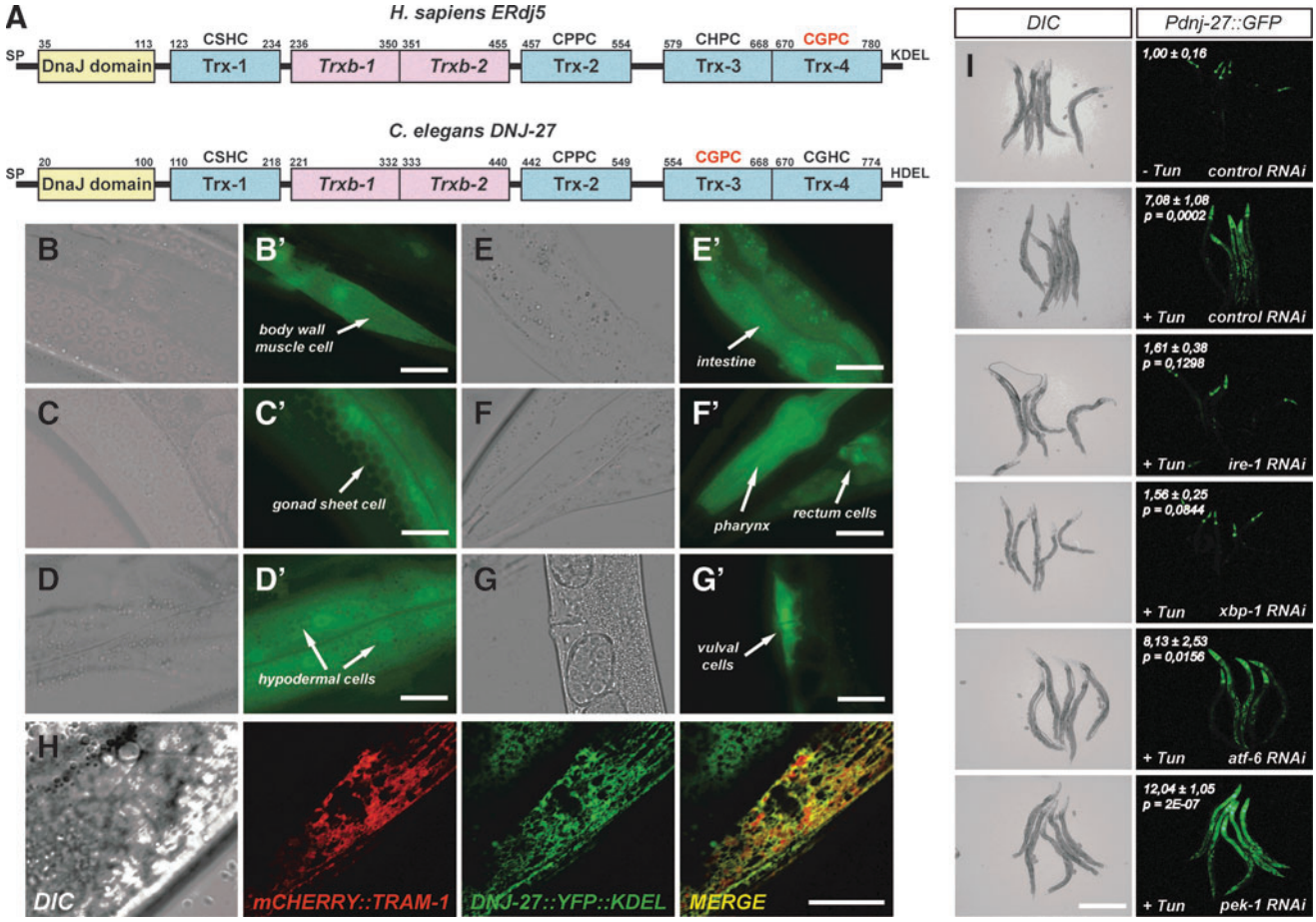

FIG. 1. Domain organization, expression pattern and induction upon tunicamycin treatment of *Caenorhabditis elegans dnj-27*. (A) Protein domain comparison between human ERdj5 and *C. elegans* DNJ-27. Numbers above the different domains denote the amino acid residue of the protein. Blue boxes indicate the thioredoxin domains containing CXXC redox active sites, while the pink boxes indicate the domains that lack any identifiable CXXC redox active site but maintain the thioredoxin fold (24). The sequence of the respective redox active sites is shown above their corresponding domains and the canonical thioredoxin active site CGPC is highlighted in red. The abbreviation Sp designates the N-terminal signal peptide, while HDEL and KDEL are the respective C-terminal tetrapeptides responsible for ER luminal retention (40). **(B–G')** Expression pattern of the strain BC10640 expressing the *Pdnj-27::GFP* transgene. Micrographs of transgenic worms were visualized with differential interference contrast optics **(B–G)** and fluorescence (B'–G'). Bar = 20 μm. **(H)** ER localization of DNJ-27::YFP::KDEL fusion protein. Transgenic animals simultaneously expressing the *vzEx91 [Pmyo-3::mCherry::tram-1]* (red channel) and *vzEx60 [Pdnj-27::dnj-27::YPF::KDEL]* (green channel) show colocalization in the lumen of the ER of body wall muscle cells, as demonstrated by the yellow color of the merged image. Bar = 20 μm. **(I)** Induction of the *Pdnj-27::GFP* transgene upon tunicamycin treatment (30 μg/ml). The induction of the fluorescence upon tunicamycin treatment is robustly downregulated in worms where signaling *via ire-1/xbp-1* (but not the *atf-6* and *pek-1*) pathway has been inhibited by RNAi. Bar = 400 μm. Fluorescence intensity of animals grown on control RNAi without tunicamycin was set to value = 1 and the intensity values of the different RNAi treatments in the presence of tunicamycin indicate the fold induction ± standard deviation compared to the control (*Left upper corner*). Unpaired two-tailed *t-test* was used to determine the statistical significance (p) of the fluorescence intensity ($n = 10$). ER, endoplasmic reticulum; GFP, green fluorescent protein; RNAi, RNA interference; YFP, yellow fluorescent protein. To see this illustration in color, the reader is referred to the web version of this article at www.liebertpub.com/ars

pattern. Thus, *Pdnj-27::GFP* is mainly expressed in pharynx and vulval cells with weaker expression in other tissues, such as body wall muscle cells, intestine, gonad sheath cells, rectum, and hypodermis (Fig. 1B–G).

Both human ERdj5 and *C. elegans* DNJ-27 proteins are flanked by an N-terminal signal peptide and by a C-terminal ER-retention signal tetrapeptide (KDEL for ERdj5 and HDEL for DNJ-27) that are required to target and retain the proteins in the ER lumen, respectively (Fig. 1A). To confirm this subcellular localization [and taking advantage of an available DNA construct encoding yellow fluorescent protein (YFP) engineered to harbor the KDEL tetrapeptide at its C-terminus (37)], we generated the reporter *Pdnj-27::dnj-27::YFP::KDEL*, that expresses DNJ-27 fused to YFP::KDEL. The KDEL tetrapeptide has been shown to be functionally similar to HDEL in yeast (40) and this seems to be the case for *C. elegans* as well, where several worm ER resident proteins containing either C-terminal tetrapeptide are found in the *C. elegans* proteome. As shown in Figure 1H, transgenic nematodes simultaneously expressing DNJ-27::YFP::KDEL (under the control of its own

promoter) and the *C. elegans* ER-marker mCherry::TRAM-1 (under the control of the *myo-3* promoter) (75) demonstrated a marked colocalization of both proteins in the muscle cells of these animals, confirming that DNJ-27 is also an ER luminal protein in *C. elegans*.

The unfolded protein response (UPR), a set of conserved intracellular signaling pathways that sense protein misfolding within the ER and work to regulate ER stress, is intimately coordinated with ERAD, which eliminates terminally misfolded non-native proteins *via* retrograde translocation and degradation in the cytosol (76). In mammals, the UPR is activated through three different pathways involving the proteins IRE1/XBP1, PERK, and ATF6 (44) (termed IRE-1, XBP-1, PEK-1, and ATF-6 in *C. elegans*). ERdj5 has been previously found to be upregulated by ER stressors that induce UPR (11). To determine whether *dnj-27* is also upregulated upon ER stress, we treated transgenic animals expressing the *Pdnj-27::GFP* reporter with tunicamycin, a typical ER stress inducer (61). Treatment with 10, 20, and 30 μg/ml tunicamycin resulted in a strong increase of GFP fluorescence (Fig. 1I and data not shown). Using RNAi, we also determined that tunicamycin-induced expression of *dnj-27* requires IRE-1/XBP-1 but is ATF-6 and PEK-1 independent, as only RNAi downregulation of *ire-1* and *xbp-1*, but not *atf-6* or *pek-1*, caused a marked decrease in the expression of the *Pdnj-27::GFP* transcriptional reporter. Indeed, *pek-1* downregulation produced a significant increase in *dnj-27* reporter expression (Fig. 1I). Inhibition of *pek-1*, but not *atf-6* or *ire-1/xbp-1*, activates the UPR in *C. elegans* (61). Therefore, a possible explanation for this effect could be that *pek-1* RNAi would lead to a further activation of the UPR, thus resulting in a higher induction of *dnj-27*. The induction of *dnj-27* through the IRE-1/XBP-1 pathway is consistent with a role of DNJ-27 in ERAD as this pathway has been specifically linked to the transcriptional induction of genes that function in ERAD, such as the ERdj5 partner EDEM (89).

Using the ER stress reporter *Phsp-4::GFP* (79), we next examined whether efficient knockdown of *dnj-27* by RNAi [demonstrated by the decreased expression of the *Pdnj-27::dnj-27::GFP* translational reporter (Supplementary Fig. S1A)] induces UPR activation. Similar to mammalian ERdj5 (80), ER stress was not induced in worms where *dnj-27* was downregulated (data not shown). Moreover, wild type animals treated with *dnj-27* RNAi showed no obvious phenotype, in consonance with the healthy and viable phenotype reported for the ERdj5 knockout mice (31). Importantly, *dnj-27* RNAi downregulation did not cause any motility defects in wild type worms as demonstrated by bending and thrashing assays (Supplementary Figs. S1B and S6).

As a whole, the high homology between ERdj5 and DNJ-27 together with the DNJ-27 ER-localization and induction upon ER-stress *via* IRE-1/XBP-1 pathway, strongly suggests that the function of *dnj-27/ERdj5* in ERAD is conserved.

dnj-27 protects against intracellular human Aβ toxicity and aggregation in a transgenic C. elegans model of AD

To evaluate whether members of the Trx family of redox proteins modulate human Aβ and α-syn aggregation, we performed an RNAi screen of all the seven *C. elegans* Trxs with the conserved active site sequence WCGPC plus the two thioredoxin reductases in transgenic worm models that express human Aβ or human α-syn::GFP in worm body wall muscle cells (Supplementary Table S2). Aβ aggregation causes an easily scored aging-dependent paralysis phenotype (43), while α-syn::GFP aggregation results in the formation of fluorescent aggregates that can be readily identified *in vivo* under a fluorescence microscope thanks to the transparency of the animal (25). As a result of this RNAi screen we identified the worm gene *dnj-27* as the only member of the Trx family playing a protective role in both models (Supplementary Table S2).

Initially, for the Aβ RNAi screen, we used the transgenic strain CL647 (Supplementary Table S1) that overproduces human Aβ in body wall muscle cells in an inducible manner after temperature upshift (from 16°C to 25°C) at the L3 larval stage, since it allows a rapid scoring of paralysis (12). This strain also carries the *rrf-3(pk1426)* mutation that hypersensitizes worms against feeding RNAi (65). However, to rule out the effect of a higher temperature on the ER-stress machinery, we decided to perform the subsequent analyses with the CL2006 strain that overexpresses the human Aβ peptide constitutively, also in body wall muscle cells (hereafter Aβ worms) (41). As shown in Figure 2A, *dnj-27* downregulation caused a significant acceleration of the onset of paralysis in Aβ worms.

To gain deeper insight into the mechanisms by which *dnj-27* exerts this protective function, we wondered whether this enhancement on the paralysis phenotype was associated with differences in the formation of Aβ aggregates. Immunohistochemistry with the fluorescent amyloid vital dye X-34 (42) on Aβ worms demonstrated that *dnj-27* RNAi induces a mild, although statistically significant, increase of amyloid deposit formation (Fig. 2B, C). To determine whether this increase of amyloid deposits was due to changes in total Aβ content or changes in the Aβ oligomeric state, we performed immunoblotting on Aβ worm extracts using the Aβ-peptide specific antibody 6E10, which detects all forms of Aβ. We found no major differences in either total Aβ levels or Aβ oligomeric species in *dnj-27* downregulated Aβ worms as compared to control animals (Fig. 2G; Supplementary Fig. S2A).

Since downregulation of *dnj-27* enhances the Aβ-dependent paralysis phenotype, we next asked whether higher levels of DNJ-27 would improve the paralysis onset. To this aim, we generated transgenic strains expressing the construct *Pdnj-27::dnj-27*, which produces high levels of DNJ-27 under the control of its endogenous *dnj-27* promoter (Supplementary Fig. S3A). Transgenic Aβ worms overexpressing *dnj-27* showed a significant reduction of the paralysis onset compared to their corresponding nontransgenic control siblings (Fig. 2D). *dnj-27* overexpressing transgenic Aβ worms also showed a strong decrease of amyloid deposits formation (Fig. 2E, F), while, similarly to *dnj-27* RNAi downregulation, total Aβ and Aβ oligomers were not significantly affected (Fig. 2G; Supplementary Fig. S2A).

Another important issue arising from our results was the evident effect of the type of food source on Aβ-induced toxicity. In RNAi experiments, animals were grown on *Escherichia* coli HT115 (an RNAi *E. coli* feeding strain), while *E. coli* OP50 (the standard laboratory food source) was used for overexpression experiments. Thus, when comparing Aβ worms grown on OP50 and HT115, we detected a much faster

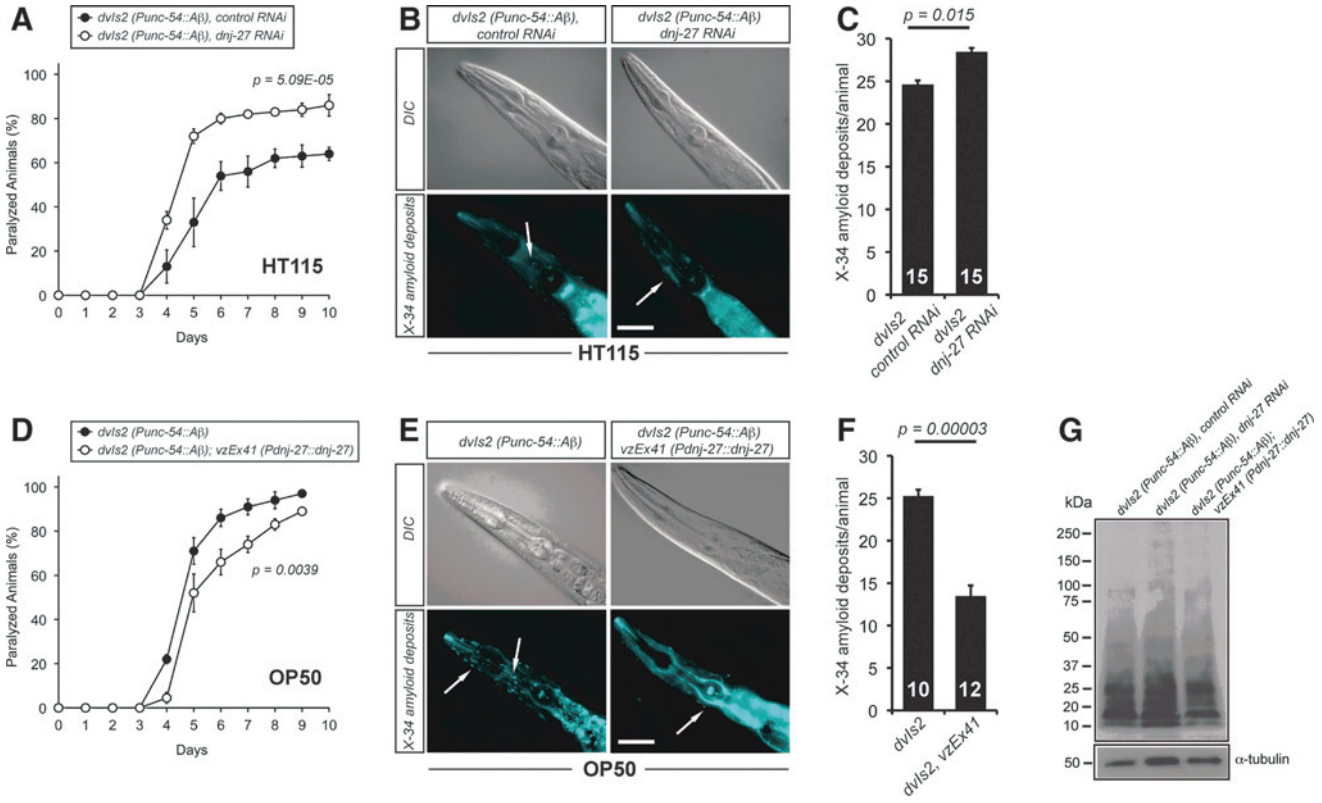

FIG. 2. Effect of downregulation or overexpression of *dnj-27* on the paralysis and Aβ deposit formation in Aβ worms. **(A)** Progressive paralysis of CL2006, *dvIs2 [Punc-54::Aβ3-42::unc-54 3′-UTR; rol-6(su1006)]* worms grown on HT115 bacteria expressing either no dsRNA (●) or *dnj-27* dsRNA (○). The graph represents the average of three independent experiments. **(B)** X-34 staining of Aβ deposits in the muscles of the head region of 1-day adult CL2006 worms grown on HT115 bacteria expressing either no dsRNA (*left panels*) or *dnj-27* dsRNA (*right panels*). *Arrows* denote the X-34 Aβ deposits. Bar = 50 μm. **(C)** Quantification of the X-34 Aβ deposits of the worms imaged in (B). The numbers in the columns denote the worms used for each RNAi treatment. **(D)** Progressive paralysis of CL2006 worms (●) and its derivative transgenic strain VZ158 carrying the extrachromosomal array *vzEx41 [Pdnj-27::dnj-27::dnj-27 3′-UTR; Punc-122::GFP]* (○) growing on OP50 bacteria. The graph represents the average of three independent experiments. **(E)** X-34 staining of Aβ deposits in the muscles of the head region of 1-day adult CL2006 worms (*left panels*) and its derivative transgenic strain VZ158 (*right panel*) grown on OP50 bacteria. *Arrows* denote the X-34 Aβ deposits. Bar = 50 μm. **(F)** Quantification of the X-34 Aβ deposits of the worms imaged in (E). The numbers in the columns denote the worms used for each strain. **(G)** Aβ immunoblot using the 6E10 monoclonal antibody. All lanes were loaded with total protein extract from 100 synchronized 1-day adult CL2006 and VZ158 worms growing on HT115 bacteria expressing no dsRNA (lanes 1 and 3 to the right of the size marker, respectively) and CL2006 worms growing on HT115 bacteria expressing *dnj-27* dsRNA (lane 2 to the right of the size marker). No differences in total amount or oligomeric Aβ species were found. α-tubulin was used as loading control. For statistical analyses, Two-way ANOVA was used in (A) and (D), while Unpaired *t-test* with two tail distribution was performed in (C) and (F). The error bars indicate the SEM. Western quantifications are shown in Supplementary Figure S2A. Aβ, beta amyloid peptide; ANOVA, analysis of variance; SEM, standard error of the mean; UTR, untranslated region. To see this illustration in color, the reader is referred to the web version of this article at www.liebertpub.com/ars

paralysis onset in the animals grown on OP50 (Fig. 2A *vs.* D, black circles), while formation of amyloid deposits remained practically the same (Fig. 2B, C *vs.* E, F). We then repeated the paralysis assays growing transgenic Aβ worms overexpressing *dnj-27* on HT115 bacteria. As expected, the paralysis phenotype was also improved in these transgenic animals. However, the paralysis onset of the *dnj-27* overexpressing worms grown on HT115 bacteria was dramatically reduced in comparison to that reached by the same animals grown on OP50 bacteria (Supplementary Fig. S4A *vs.* Fig. 2D, white circles).

Overall, these data indicate that *dnj-27* plays an *in vivo* protective role on Aβ toxicity and amyloid deposit formation in *C. elegans*.

dnj-27 protects against intracellular human α-syn toxicity and aggregation in different transgenic C. elegans models of PD

Next, we set to quantify the effect of *dnj-27* on α-syn toxicity and aggregation. Intracytoplasmic α-syn inclusions, called Lewy bodies, are the characteristic hallmark of PD and other synucleinopathies (67). *C. elegans* models of PD that recapitulate distinct aspects of this ND upon human α-syn expression in body wall muscle cells and dopaminergic (DA) neurons have been developed (25, 82).

Initially, for the α-syn RNAi screen, we used the transgenic strain UA50 (Supplementary Table S1) that overproduces the fusion protein α-syn::GFP along with TOR-2 in worm

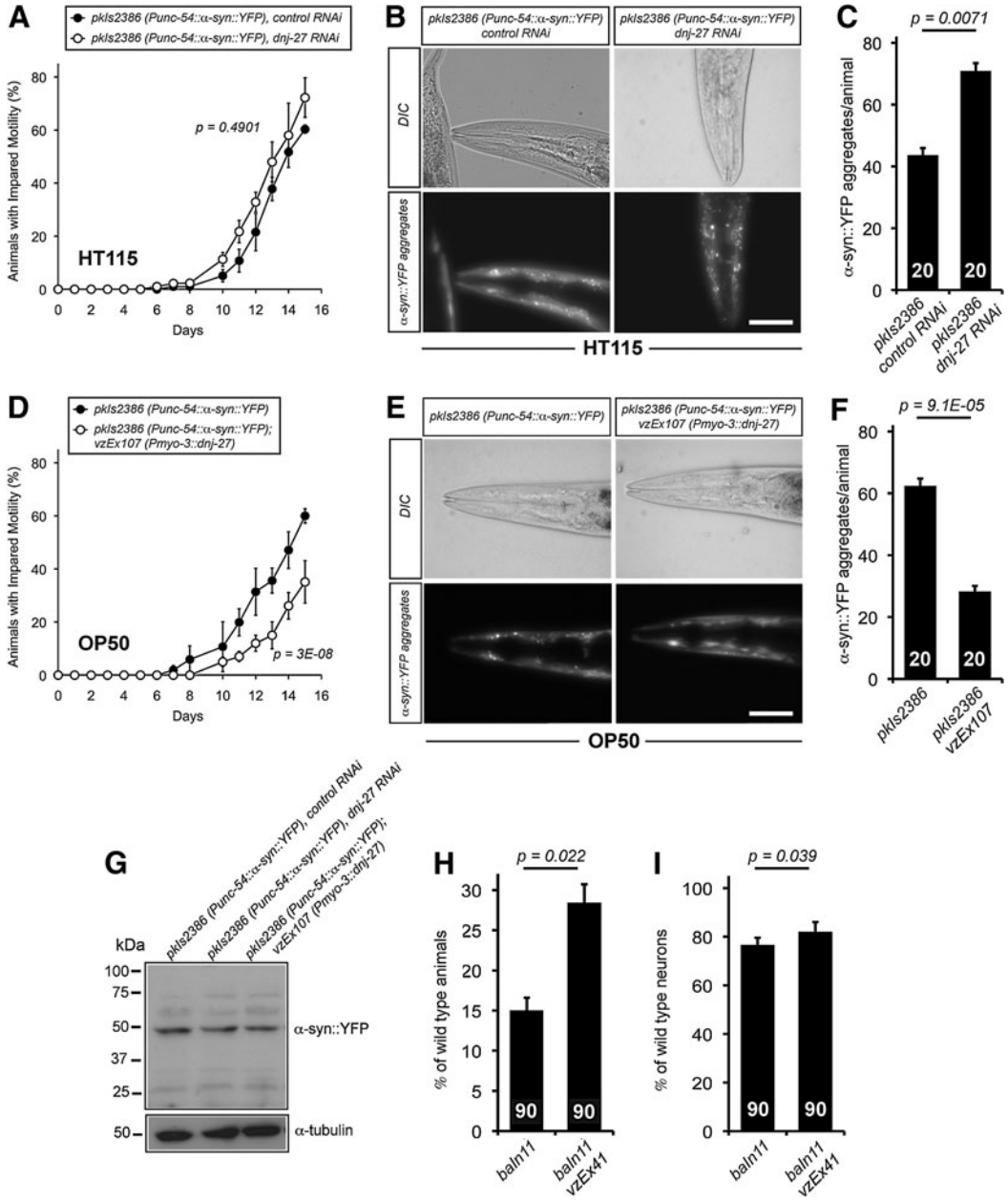

FIG. 3. Effect of downregulation or overexpression of *dnj-27* on the mobility and α-syn::YFP aggregation in α-syn worms. (A) Impaired mobility of NL5901, *pkIs2386 [Punc-54::α-syn::YFP::unc-54 3′-UTR; unc-119 (+)]* worms grown on HT115 bacteria expressing either no dsRNA (●) or *dnj-27* dsRNA (○). The graph represents the average of three independent experiments. **(B)** α-syn::YFP aggregation in the muscles of the head region of 1-day adult NL5901 worms grown on HT115 bacteria expressing either no dsRNA (*left panels*) or *dnj-27* dsRNA (*right panels*). Bar = 50 μm. **(C)** Quantification of the α-syn::YFP aggregates of the worms imaged in (B). The numbers in the columns denote the worms used for each RNAi treatment. **(D)** Impaired mobility of NL5901 worms (●) and its derivative transgenic strain VZ303 (○) grown on OP50 bacteria. The graph represents the average of three independent experiments. **(E)** α-syn::YFP aggregation in the muscles of the head region of 1-day adult NL5901 worms (*left panel*) and its derivative transgenic strain VZ303 (*right panel*) grown on OP50 bacteria. Bar = 50 μm. **(F)** Quantification of the α-syn::YFP aggregation of the worms imaged in (E). The numbers in the columns denote the worms used for each strain. **(G)** α-syn::YFP immunoblot using an anti-GFP antibody. All lanes were loaded with total protein extract from 100 synchronized 1-day adult NL5901 worms and its derivative transgenic strain VZ303 carrying the extrachromosomal array *vzEx107 [Pmyo-3::dnj-27 cDNA::unc-54 3′-UTR; Ptrx-3::mCherry]*, grown on HT115 bacteria expressing no dsRNA (lanes 1 and 3 to the right of the size marker, respectively) and NL5901 worms growing on HT115 bacteria expressing *dnj-27* dsRNA (lane 2 to the right of the size marker). No differences in total amount of α-syn::YFP were found. α-tubulin was used as loading control. **(H)** Percentage of UA44, *baIn1 [Pdat-1::α-syn::unc-54 3′-UTR; Pdat-1::GFP]* worms and its derivative transgenic strain VZ199 carrying the extrachromosomal array *vzEx41 [Pdnj-27::dnj-27::3′-UTR dnj-27; Punc-122::GFP]* that had the full complement of six anterior dopaminergic neurons at day 7. The numbers in the columns denote the worms used for each strain. The graph represents the average of three independent experiments. **(I)** Percentage of intact dopaminergic neurons per worm scored at day 7 for UA44 worms and its derivative transgenic strain VZ199. The numbers in the columns denote the worms used for each strain. The graph represents the average of three independent experiments. For statistical analyses, Two-way ANOVA was used in (A) and (D), while Unpaired *t-test* with two tail distribution was performed in (C), (F), (H) and (I). The error bars indicate the SEM. Western quantifications are shown in Supplementary Figure S2B. α-syn, alpha-synuclein.

body wall muscle cells. TOR-2 ameliorates the formation of α-syn::GFP aggregates, thus facilitating the identification of aggregation enhancers in RNAi screens (25). However, for the subsequent analyses we used the *C. elegans* strain NL5901 that overexpresses α-syn::YFP within worm body wall muscle cells (hereafter called α-syn worms). This strain exhibits age-dependent mobility defects associated with α-syn::YFP aggregation, which can be easily monitored (81,82). As shown in Figure 3A, an increase in the percentage of animals with impaired mobility was observed in α-syn worms upon *dnj-27* RNAi downregulation, although the differences were not statistically significant. In contrast, decreased levels of *dnj-27* clearly worsen α-syn::YFP aggregation (Fig. 3B, C) without affecting the total α-syn::YFP levels (Fig. 3G; Supplementary Fig. S2B).

Similarly to Aβ worms, we next aimed to determine whether *dnj-27* overexpression would protect from α-syn::YFP toxicity and aggregation in *C. elegans*. To this end, α-syn worms also expressing the *Pdnj-27::dnj-27* construct were generated. However, the results obtained with this strain were not reproducible and we decided to force the expression of DNJ-27 in body wall muscle cells by using the *myo-3* promoter (Supplementary Fig. S3B). Transgenic α-syn worms overexpressing *dnj-27* in muscle cells showed a clear improvement in mobility compared to nontransgenic control animals (Fig. 3D). Moreover, the reduction in α-syn::YFP toxicity was accompanied by a strong decrease in α-syn::YFP aggregates (Fig. 3E, F), while no changes in total α-syn::YFP levels were observed (Fig. 3G; Supplementary Fig. S2B).

Differences in toxicity between α-syn worms grown on HT115 or OP50 were not as obvious as for Aβ worms (compare Fig. 3A, D, black circles for α-syn worms and Supplementary Figs. S4B and Fig. 3D, white circles, for α-syn worms overexpressing *dnj-27*). Nonetheless, α-syn::YFP aggregation was clearly higher in α-syn animals grown on OP50 than on HT115 (62 aggregates/worm in OP50 *vs.* 43 in HT115) (Fig. 3C, F).

DA neurons are the main neuronal type affected in PD (67). We next set to determine whether *dnj-27* protection could also be extrapolated to a *C. elegans* model of DA neurodegeneration induced by α-syn (7). For this purpose, we used the strain UA44 that expresses human α-syn in DA under the control of the dopamine transporter *dat-1* promoter and that causes an age-dependent DA neurodegeneration (7, 10). DA neurons are easily identified by the simultaneous expression of GFP under the control of the *dat-1* promoter. Thus, animals overexpressing *dnj-27* under the control of its own promoter were analysed for evidence of degenerative changes in DA neurons. Higher levels of DNJ-27 significantly improved both the percentage of animals with the normal number of neurons (Fig. 3H) and the percentage of total nondegenerated neurons (Fig. 3I). Together, our data indicate that *dnj-27* is protective against α-syn dependent deleterious phenotypes.

dnj-27 protection is also extended to the toxicity associated to polyQ aggregation in C. elegans

To investigate the protective role of *dnj-27* in other aggregation-prone proteins, we resorted to a previously developed *C. elegans* model of CAG-repeat disorders (47). The expression of either GFP or YFP fused to different numbers of glutamine residues in *C. elegans* body wall muscle cells leads to polyQ-dependent aggregation and toxicity when the number of glutamine expansions is greater than 35–40 residues (47, 49). In this work, we used the AM141 strain which shows mobility impairment upon expression of Q40::YFP in body wall muscle cells (referred to as Q40 worms hereafter) (47).

First, we studied the effect of knocking down *dnj-27* by RNAi on the mobility of the AM141 strain. As shown in Figure 4A, decreased levels of DNJ-27 resulted in a higher percentage of animals with impaired mobility, accompanied by a striking fourfold increase in the number of Q40::YFP aggregates (Fig. 4B, C). Similarly to Aβ and α-syn worms, we performed immunoblotting on Q40 worms using anti-GFP antibodies (which efficiently cross-react with YFP) to rule out that *dnj-27* inhibition could be affecting the total Q40::YFP levels. As shown in Figure 4G and Supplementary Figure S2C, total Q40::YFP levels were not affected by *dnj-27* downregulation.

On the contrary, overexpression of *dnj-27* in body wall muscle cells did not improve the impaired mobility associated with Q40 animals when DNJ-27 transgenic worms were compared to their corresponding nontransgenic control siblings (Fig. 4D; Supplementary Fig. S4C), although a statistically significant decrease in the number of aggregates was observed (Fig. 4E, F).

Our results highlight that Q40-dependent toxicity and aggregation are also influenced by the type of food source, as demonstrated in the Aβ model (Fig. 2). Thus, compared to animals grown on HT115, Q40 worms grown on OP50 show a strong increase in both the percentage of animals with impaired mobility (Fig. 4A; Supplementary Fig. S4C *vs.* Fig. 4D black circles) and in the numbers of aggregates (79 aggregates/worm on OP50 *vs.* 5 on HT115) (Fig. 4B, C *vs.* E, F).

As a whole, these data demonstrate a general *in vivo* protective role of *dnj-27* on Aβ, α-syn and Q40-dependent toxicity and aggregation in *C. elegans*.

ERdj5, the mammalian ortholog of dnj-27, is also protective in some of the C. elegans ND models

To determine whether the protective effects of *dnj-27* described above are conserved across evolution, we overexpressed human *ERdj5*, the mammalian ortholog of *dnj-27*, in the body wall muscle cells of the three various worm models of ND. For Aβ worms we evaluated the paralysis phenotype and, in contrast to *dnj-27* overexpressing Aβ worms, we found no improvement of the paralysis onset in worms expressing human ERdj5 (Supplementary Fig. S5). However, it should be noted that overexpression of human ERdj5 in Aβ animals caused a severe embryonic and larval arrest phenotype. Given that the paralysis assay is performed in adult worms, it is plausible that the animals selected for the assay were those segregants expressing the lowest levels of ERdj5, thus explaining the lack of paralysis rescue. In contrast, for the other two models, we found a significant decrease in the number of α-syn::YFP and Q40::YFP aggregates when ERdj5 was overexpressed (Fig. 5B, C, E, F). Regarding toxicity, and similarly to DNJ-27 overexpression, human ERdj5 was protective against α-syn toxicity (Fig. 5A), while it had no such effect in the Q40 animals (Fig. 5D). In summary, our results show that the protective role of *dnj-27* in alleviating cytoplasmic proteostasis is recapitulated (at least in the α-syn and Q40 models) by human ERdj5, further supporting *dnj*-27 as the ortholog of

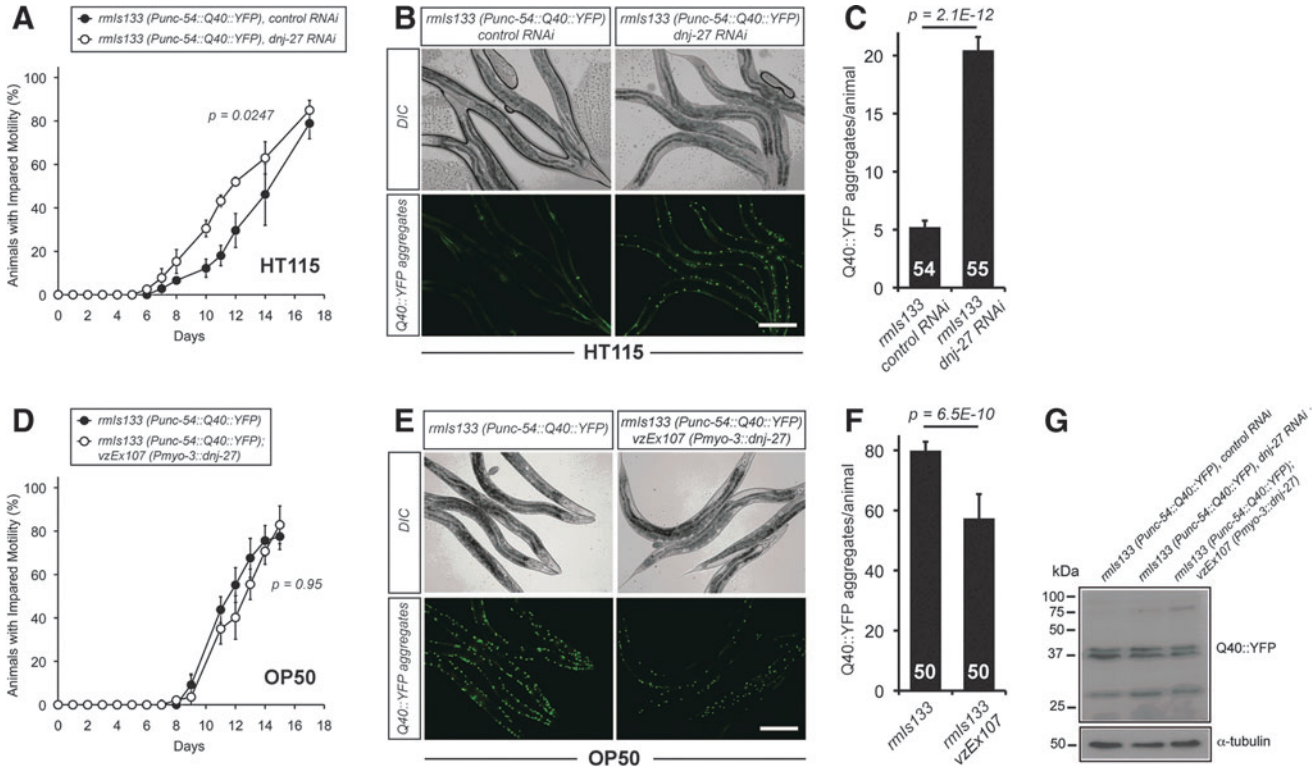

FIG. 4. Effect of downregulation or overexpression of *dnj-27* on the mobility and Q40::YFP aggregation in Q40 worms. **(A)** Impaired mobility of AM141, *rmIs133 [Punc-54::Q40::YFP::unc-54 3′-UTR]* worms grown on HT115 bacteria expressing either no dsRNA (●) or *dnj-27* dsRNA (○). The graph represents the average of three independent experiments. **(B)** Q40::YFP aggregation in the body wall muscle cells of 1-day adult AM141 worms grown on HT115 bacteria expressing either no dsRNA (*left panels*) or *dnj-27* dsRNA (*right panels*). Bar = 200 μm. **(C)** Quantification of the Q40::YFP of the worms imaged in (B). The numbers in the columns denote the worms used for each RNAi treatment. **(D)** Impaired mobility of AM141 worms (●) and its derivative transgenic strain VZ299 carrying the extrachromosomal array *vzEx107 [Pmyo-3::dnj-27 cDNA::unc-54 3′-UTR; Ptrx-3::mCherry]* (○) growing on OP50 bacteria. The graph represents the average of two independent experiments. **(E)** Q40::YFP aggregation in the body wall muscle cells of 1-day adult AM141 worms (*left panels*) and its derivative transgenic strain VZ299 (*right panel*) grown on OP50 bacteria. Bar = 200 μm. **(F)** Quantification of the Q40::YFP aggregated of the worms imaged in (E). The numbers in the columns denote the worms used for each strain. **(G)** Q40::YFP immunoblot using an anti-GFP antibody. All lanes were loaded with total protein extract from 100 synchronized 1-day adult AM141 and VZ299 worms grown on HT115 bacteria expressing no dsRNA (lanes 1 and 3 to the right of the size marker, respectively) and AM141 worms grown on HT115 bacteria expressing *dnj-27* dsRNA (lane 2 to the right of the size marker). No differences in total amount of Q40:YFP were found. The double band identified by the anti-GFP antibody most likely reflects proteolytic cleavage of Q40::YFP. α-tubulin was used as loading control. For statistical analyses, Two-way ANOVA was used in (A) and (D), while Unpaired *t-test* with two tail distribution was performed in (C) and (F). The error bars indicate the SEM. Western quantifications are shown in Supplementary Fig. S2C. cDNA, complementary DNA. To see this illustration in color, the reader is referred to the web version of this article at www.liebertpub.com/ars

ERdj5 and suggesting a potential protective role of ERdj5 in human ND pathologies.

Other C. elegans ERAD genes are also protective in models of ND

ER misfolded proteins to be degraded by the ERAD pathway transit through different steps that entail substrate recognition, targeting, retrotranslocation, ubiquitination, and proteasomal degradation (84). Among these steps, the supramolecular functional ERAD complex formed by EDEM and ERdj5 is implicated in the substrate recognition and targeting steps (84).

Previously described *C. elegans* ERAD genes include *cup-2* and *R151.6*, which encode Derlin proteins and are candidates for the retrotranslocation channel (59, 60, 88); *sel-1*, ortholog of human *sel1* (79), a member of the HRD complex that degrades misfolded ER-resident proteins (26); *sel-11/hrd-1* and *hrdl-1*, two E3 ubiquitin ligases (57) and *cdc-48.1* and *cdc-48.2*, orthologues of human *p97* that functions as a ubiquitin-selective chaperone (48). Thus, *cup-2* and *R151.6* are part of the retrotranslocation step, *sel-1*, *sel-11/hrd-1* and *hrdl-1* would be involved in ubiquitination, while *cdc-48.1* and *cdc-48.2* would be implicated in proteasomal targeting and degradation.

To determine whether these other ERAD genes, similarly to *dnj-27*, would also affect the aggregation and toxicity of aggregation-prone proteins in the cytoplasm, we studied the effect of downregulating these genes by RNAi on the paralysis of Aβ worms as well as on polyQ aggregation. Control RNAi downregulation of these genes in wild type worms does not cause any motility phenotype as demonstrated by a thrashing assay (Supplementary Fig. S6). As shown in Table 1, we found an enhancement of the paralysis phenotype of Aβ worms as well as an increase in polyQ

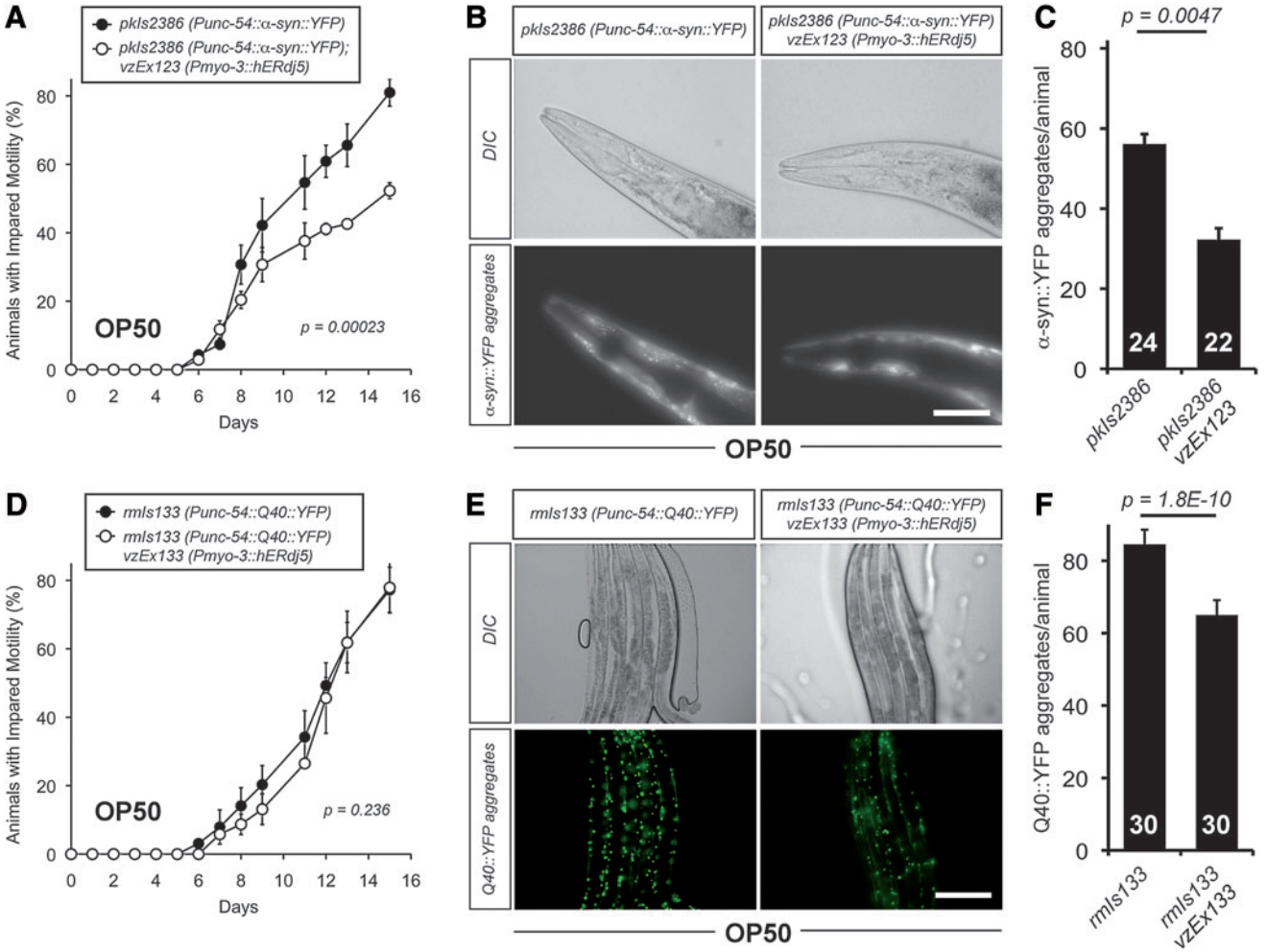

FIG. 5. Effect of overexpressing human *ERdj5* on the paralysis and aggregation phenotype in α-syn and Q40 worms. (A) Impaired mobility of NL5901, *pkIs2386 [Punc-54::α-syn::YFP::unc-54 3′-UTR; unc-119 (+)]* worms (●) and its derivative transgenic strain VZ316 carrying the extrachromosomal array *vzEx123 [Pmyo-3::hERdj5 cDNA::unc-54 3′-UTR; Punc-122::GFP]* (○) grown on OP50 bacteria. The graph represents the average of two independent experiments. **(B)** α-syn::YFP aggregation in the muscles of the head region of 1-day adult NL5901 worms (*left panels*) and its derivative transgenic strain VZ316 (*right panel*) grown on OP50 bacteria. Bar = 50 μm. **(C)** Quantification of the α-syn::YFP aggregation of the worms imaged in (B). The numbers in the columns denote the worms used for each strain. **(D)** Impaired mobility of AM141, *rmIs133 [Punc-54::Q40::YFP::unc-54 3′-UTR]* worms (●) and its derivative transgenic strain VZ363 carrying the extrachromosomal array *vzEx133 [Pmyo-3::hERdj5 cDNA::unc-54 3′-UTR; Pmyo-2::mCherry]* (○) grown on OP50 bacteria. The graph represents the average of two independent experiments. **(E)** Q40::YFP aggregation in the body wall muscle cells of 1-day adult AM141 worms (*left panel*) and its derivative transgenic strain VZ363 (*right panel*) grown on OP50 bacteria. Bar = 200 μm. **(F)** Quantification of the Q40::YFP aggregates of the worms imaged in (E). The numbers in the columns denote the worms used for each strain. For statistical analyses, Two-way ANOVA was used in (A) and (D), while Unpaired *t-test* with two tail distribution was performed in (C) and (F). The error bars indicate the SEM. To see this illustration in color, the reader is referred to the web version of this article at www.liebertpub.com/ars

aggregation in four out of the five ERAD genes tested. It is worth noting that a RNAi screen performed by Nollen *et al.* in polyQ worms found no effect in polyQ aggregation when downregulating *dnj-27* or any of the genes studied in Table 1 (49). This apparent discrepancy can be explained by two facts: (i) the study by Nollen *et al.* was performed in animals grown for one generation on the respective RNAi, while our work used animals grown for two generations on the respective RNAi to ensure effective gene downregulation and (ii) the screen by Nollen *et al.* used Q35::YFP animals in which the polyQ stretches cause an intermediate aggregation phenotype, while our study uses Q40::YFP worms where the polyQ stretches produce a more severe aggregation phenotype (49).

We also mined data from two published RNAi screens in *C. elegans* whereby modulation of α-syn aggregation was assessed (25, 82). There were some differences in identified modifiers between these distinct studies, likely because they employed different genetic backgrounds. Specifically, Hamamichi *et al.* (25) utilized a transgenic background wherein α-syn misfolding was attenuated with a chaperone concurrent to RNAi treatment, while van Ham *et al.* (82) screened for enhanced α-syn aggregation in nonattenuated backgrounds. Importantly, when these two screens are combined, four out

Table 1. Effect of RNAi Downregulation of ERAD Genes on the Paralysis Phenotype of *CL*2006 Strain and Aggregation Phenotype of *UA*50, *NL*5901 and *AM*141 Strains

Gene name	*Human ortholog*	*Function in the ER*	*Effect on paralysis of CL2006 (Punc-54::Aβ) [this study]*	*Effect on aggregation of UA50 (Punc-54::α-syn::GFP + Punc-54:: tor-2) (25) or NL5901 (Punc-54::α-syn::YFP) (82)*	*Effect on aggregation of AM141 (Punc-54::Q40::YFP) [this study]*
sel-1/sup-25	*SEL1L*	Member of the HMG-CoA reductase degradation (HRD) complex	+	Not assayed	+
sel-11/hrd-1	*SYVN1*	E3 ubiquitin ligase	Synthetic lethality	No effect (UA50) Not assayed (NL5901)	Synthetic lethality
hrdl-1	*AMFR*	E3 ubiquitin ligase like	+	+ + (UA50) No effect (NL5901)	+ +
cup-2	*DERL1*	Derlin	+ +	Not assayed (UA50) No effect (NL5901)	+
R151.6	*DERL2*	Derlin like	+ +	No effect (UA50) + + (NL5901)	+ +

+, moderate enhancement of the phenotype.
+ +, strong enhancement of the phenotype.
ER, endoplasmic reticulum; ERAD, ER-associated degradation; GFP, green fluorescent protein; RNAi, RNA interference; YFP, yellow fluorescent protein.

of the five ERAD candidates were examined in these studies but only two of the candidates enhanced the α-syn aggregation phenotype (*hrdl-1* and *R151.6*). We therefore conclude from these studies that α-syn aggregation does not result from the knockdown of all ERAD components, since RNAi of *sel-11* and *cup-2* does not cause any enhancement of the aggregation phenotype (Table 1).

The proteasomal targeting and degradation genes, *cdc-48.1* and *cdc-48.2*, could not be targeted for RNAi as their downregulation causes embryonic and larval lethality. However, it has been reported that overexpression of either *cdc-48.1* or *cdc-48.2* suppresses the formation of polyQ aggregates in *C. elegans* (87), which also suggests a protective role of these ERAD genes in this model.

dnj-27 inhibition induces proteosomal and autophagic dependent cytoplasmic protein degradation and mitochondrial fragmentation

To get insight into the mechanisms behind the increased cytoplasmic aggregation of A*β*, α-syn::YFP, and Q40::YFP upon *dnj-27* downregulation, we aimed to determine whether *dnj-27* RNAi affects the homeostasis of the cytoplasm. Previous studies have demonstrated that ERdj5 accelerates ERAD by reducing disulfide bonds in misfolded glycoproteins (24, 80). Therefore, it is reasonable to propose that inhibiting *dnj-27* function will lead to an increase in the ER load of misfolded proteins. To alleviate this stress, an increased retrotranslocation of these misfolded proteins from the ER to the cytoplasm would happen. This, in turn, would raise the load of misfolded proteins in the cytoplasm meddling the cytoplasmic folding machinery and proteostasis (22).

To test this hypothesis, we used worms expressing a *Punc-54::LacZ* transgene which can be used as a reporter of protein degradation and proteostasis in the cytoplasm of body wall muscle cells (90). Muscle cells have a well-defined network of signals which modulate protein degradation (38), thus allowing direct testing of the relevance of these pathways to pathology. Because LacZ is synthesized only until adulthood and remains stable for at least the first 72 h of adulthood (90), it can be used to determine if acute experimental manipulations in adult muscle, for example RNAi treatment (62), trigger increased degradation. Thus, LacZ transgenic animals were grown on *dnj-27* RNAi and the LacZ reporter protein was assessed. As shown in Figure 6A, *dnj-27* downregulation promotes cytosolic protein degradation, indicating that *dnj-27* modulates cytoplasmic protein homeostasis in otherwise wild type healthy animals. Moreover, we were able to determine that the increase in degradation is related to autophagy since it was blocked by reduction-of-function mutations in genes such as *unc-51* (a serine/threonine protein kinase orthologous to *Saccharomyces cerevisiae* autophagy protein Atg1p and the vertebrate ULK proteins), *mpk-1* (a mitogen-activated protein kinase, ortholog of ERK), and *daf-18* (a lipid phosphatase, orthologous to the human PTEN tumor suppressor) (Fig. 6A). These three genes are key components of diverse signaling pathways that have been shown to modulate autophagy in *C. elegans* muscle (71, 72). Similarly, the proteasome inhibitor MG132, which has previously been shown to block proteasome mediated degradation in *C. elegans* muscle (14), was also effective in blocking the increased cytosolic protein degradation upon *dnj-27* downregulation. However, this increase was not dependent on the apoptotic pathway as it was not blocked by a loss-of-function mutation in the caspase *ced-3* (Fig. 6A).

Since toxicity was scored by means of paralysis and impaired mobility phenotypes in most cases, this raised the possibility that *dnj-27* was affecting muscle development and maintenance. However, we ruled out this possibility as we checked myofibrillar structure upon *dnj-27* RNAi downregulation using a *Pmyo-3::GFP* transgene and no myofibrillar structural changes were observed (Fig. 6B). The absence of muscle function alteration upon *dnj-27* downregulation is further supported by the lack of phenotype in bending and thrashing assays (Supplementary Figs. S1B and S6).

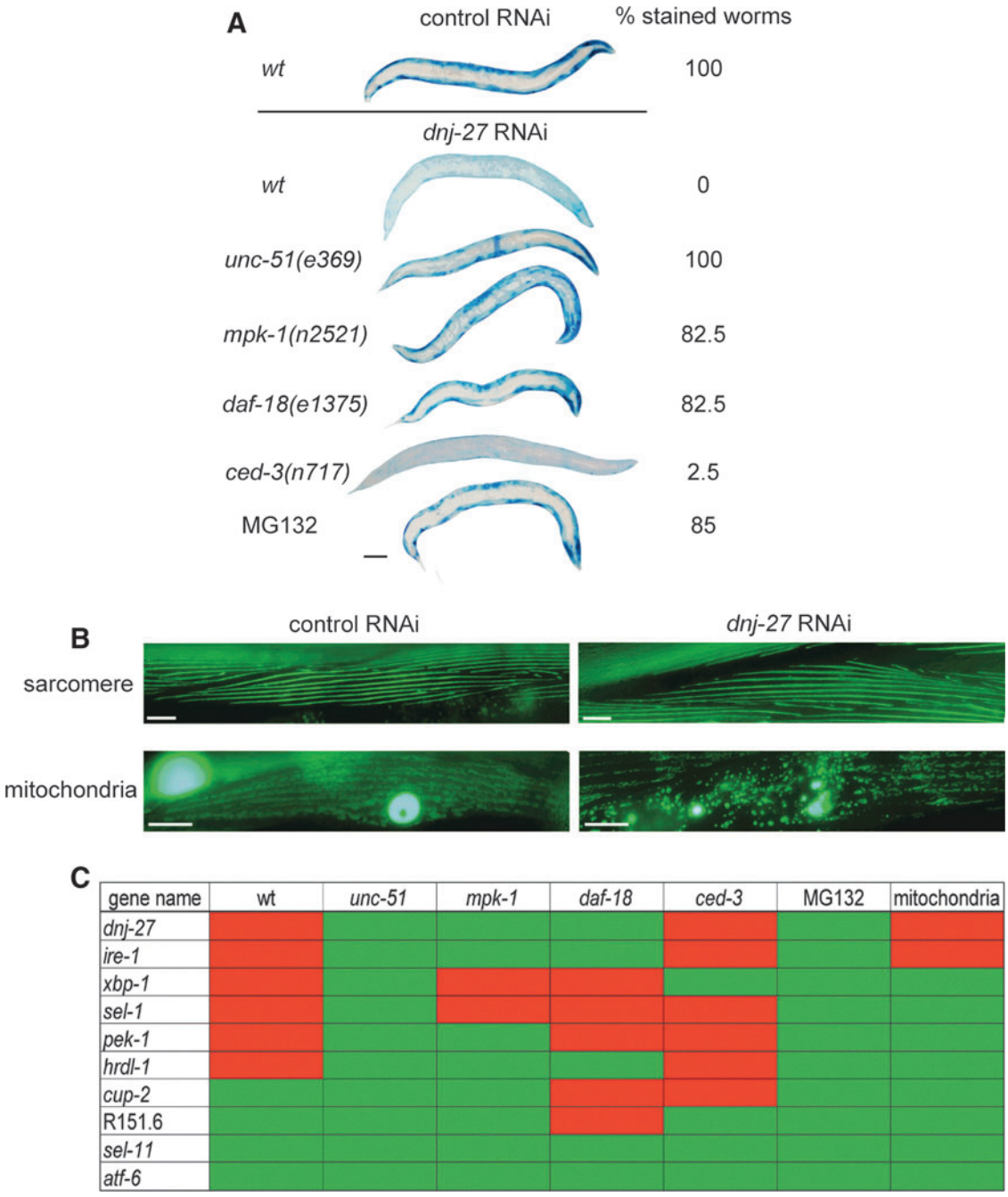

gene name	wt	*unc-51*	*mpk-1*	*daf-18*	*ced-3*	MG132	mitochondria
dnj-27							
ire-1							
xbp-1							
sel-1							
pek-1							
hrdl-1							
cup-2							
R151.6							
sel-11							
atf-6							

FIG. 6. ***dnj-27* downregulation enhances cytoplasmic protein degradation and mitochondrial fragmentation. (A)** Treatment of adult worms containing the transgenic reporter *ccIs55 [sup-7(st5); Punc-54::unc-54::lacZ]* for protein degradation (90) with RNAi against *dnj-27* for 72 h induces degradation of this reporter in a wild-type or *ced-3* mutant background. Degradation is not observed or marginally detected in an *unc-51*, *mpk-1*, or *daf-18* mutant background or in worms treated with the proteasome inhibitor MG132. The percentage of stained worms indicate the consensus result from two independent experiments each $n = 20–30$. Bar = 100 μm. **(B)** Treatment of adult worms containing GFP labeled sarcomeres (*jIs01* [*Pmyo-3::myo-3::GFP; rol-6*(*su1006*)]) (19) or mitochondria and nuclei (*ccIs4251 [Pmyo-3::nuclearGFP::lacZ; Pmyo-3::mitoGFP]*) (15, 62) with RNAi against *dnj-27* for 72 h induces no defects in sarcomere structure (*top*) but does induce fragmentation of the mitochondrial network (*bottom*). Bars = 10 μm. **(C)** Graphic representation of results for protein degradation and mitochondrial structure in response to RNAi against ER genes. Adult worms containing the same transgenic reporters as in (A) and (B) were treated with RNAi against the indicated gene (*left*). Observation of protein degradation (red) or no protein degradation (green) in wt or in the same mutant animals as in (A) are depicted (genotypes are indicated at the top of columns). Observation of fragmentation of mitochondrial networks (red) or no fragmentation of mitochondrial networks (green) is also depicted (column labeled mitochondria). Displayed data indicate the consensus result from three independent experiments each $n = 60$. To see this illustration in color, the reader is referred to the web version of this article at www.liebertpub.com/ars

Besides affecting their aggregation, *dnj-27* could be influencing the toxicity of aggregation-prone proteins by other ways. For instance, mitochondrial deficits are key events in most ND (54, 68) and have also been related to pathological phenotypes in *C. elegans* models of ND (6, 35, 86). Indeed, increased mitochondrial fragmentation has been reported in Aβ and α-syn worm models (17, 23, 32). In polyQ worm models, although no direct evidence of mitochondrial fragmentation has been reported, downregulation of the mitochondria fission *drp-1* gene improves the motility of polyQ worms (86). Furthermore, ER and mitochondria are known to be in direct contact. Biochemical studies have revealed that they both are physically connected through a specialized subcompartment called the mitochondria-associated membrane (MAM) (83), which supports bidirectional communication regulating fundamental physiological processes between these two organelles (30, 64, 70). Therefore, we wondered whether *dnj-27* RNAi would have any impact on mitochondrial structure and integrity. As shown in Figure 6B, a *Pmyo-3::MitGFP* transgene (that expresses a fusion protein of the mitochondrial targeting sequence of chicken aspartate aminotransferase and GFP in worm muscle cells under the control of the *myo-3* gene promoter) allowed us to determine that, indeed, *dnj-27* downregulation induces mitochondrial fragmentation in these cells.

Next, to determine whether this effect in cytosolic degradation and mitochondrial network is specific for *dnj-27* downregulation or, instead, is a more general consequence of compromising ER function, RNAi of other genes involved in ERAD and UPR was performed in the LacZ and mitochondrial reporter strains. Interestingly, the downregulation of some, but not all, of UPR/ERAD genes resulted in an increase of protein degradation as shown in Figure 6C. Increased protein degradation resulted from the knockdown of *ire-1*, *xbp-1*, *pek-1*, *sel-,1* and *hrdl-1*. However, knockdown of *atf-6*, *cup-2*, *R151.6* and *sel-11/hrd-1* did not increase protein degradation, maybe due to functional redundancy with other genes. In addition to *dnj-27*, only *ire-1* downregulation was shown to affect mitochondrial integrity.

Collectively, our data demonstrate a requirement of DNJ-27 for the maintenance of protein homeostasis in the cytosol, most likely as a consequence of an increased load of misfolded proteins retrotranslocated from the ER when *dnj-27* function is compromised, which also appears to affect mitochondrial network integrity.

dnj-27 modulates the mitochondrial fragmentation phenotypes of C. elegans models of ND

To further evaluate the impact of *dnj-27* in the mitochondrial network of ND worms, we generated transgenic strains expressing a fusion protein of *C. elegans* mitochondrial import receptor subunit TOMM-20 and mRFP in body wall muscle cells (a kind gift of Dr. Amir Sapir) (6) in the background of the three ND worm models. This way, we avoid overlapping with the green fluorescence derived of α-syn::YFP and Q40::YFP fusion proteins by labeling the mitochondrial network with red fluorescence.

As shown in Figure 7A, we confirmed a severe disruption of the mitochondrial network in Aβ worms, while α-syn worms displayed a milder mitochondrial fragmentation phenotype, as previously reported (17, 23, 32). Interestingly, we demonstrate for the first time that the mitochondrial network of Q40 animals is also dramatically disrupted (Fig. 7A). Moreover, *dnj-27* RNAi downregulation increased the mitochondrial fragmentation of wild type animals (Fig. 7A, B) as well as α-syn worms (Fig. 7A, C). However, the severe disruption of the mitochondrial network in Aβ and Q40 worms precluded any quantification of the effect of *dnj-27* downregulation in these two models.

Next, we set to determine whether increased levels of DNJ-27 would result in any improvement of the mitochondrial fragmentation phenotypes of the ND worms. For this purpose, we generated derivatives of Aβ and α-syn worms carrying the mitochondrial mRFP reporter and overexpressing DNJ-27 in body wall muscle cells (we were unsuccessful to generate the corresponding Q40 derivative strains; this precluded the assessment of DNJ-27 in rescuing the mitochondrial fragmentation phenotype of Q40 worms) (Supplementary Table S1). High levels of DNJ-27 strongly reduced the mitochondrial fragmentation in both Aβ and α-syn worms (Fig. 7D, E). We conclude that DNJ-27 levels modulate the mitochondrial network integrity at least in the Aβ and α-syn models, providing a possible mechanism for the protective function of *dnj-27/ERdj5* in AD and PD.

Discussion

Cells have developed elaborate protein quality-control systems to assure the maintenance of proteostasis. Within the crowded cellular environment, proteins are always at risk of misfolding. Furthermore, cellular protein homeostasis is continuously challenged by changing genetic and environmental factors, as during pathology. For instance, aberrant protein deposition, that has been shown to influence the initiation and progression of many aging-associated ND (56), is known to challenge the proteostasis network. A key component of this complex protective network is the ER, wherein quality-control mechanisms assure proper folding of all secretory and integral proteins, in such a way, that unrefoldable non-native proteins are degraded by the ERAD pathway (36).

In this study we have identified *dnj-27*, the *C. elegans* ortholog of the ERAD mammalian gene *ERdj5* (80), as a protective gene in three different nematode models of ND caused by cytoplasmic proteotoxicity. We first demonstrated that *C. elegans dnj-27* gene encodes a protein that is targeted to ER luminal space *in vivo*, as suggested by its ER-retention signal (HDEL) at the C-terminus. Moreover, *dnj-27* was induced upon ER-stress caused by tunicamicyn and this induction occurs *via* IRE-1/XBP-1 pathway, one of the three branches of the UPR. Interestingly, the transcriptional induction of EDEM, and other genes involved in ERAD, is specifically mediated by IRE-1/XBP-1 (89), strongly suggesting an evolutionarily conserved role of *ERdj5/dnj-27* in ERAD.

We have shown that DNJ-27 plays a protective role in the cytoplasmic aggregation of human Aβ, α-syn, and polyQ proteins in *C. elegans* body wall muscle cells, results that were corroborated, to some extent, when human ERdj5 was expressed in these models. These data raise the question of how DNJ-27, an ER-resident protein, is able to influence the aggregation state of aggregation-prone proteins in a different subcellular compartment, such as the cytoplasm. Indeed, *dnj-27* knockdown results in an alteration of protein homeostasis in the cytoplasm, inferred by the increased cytoplasmic

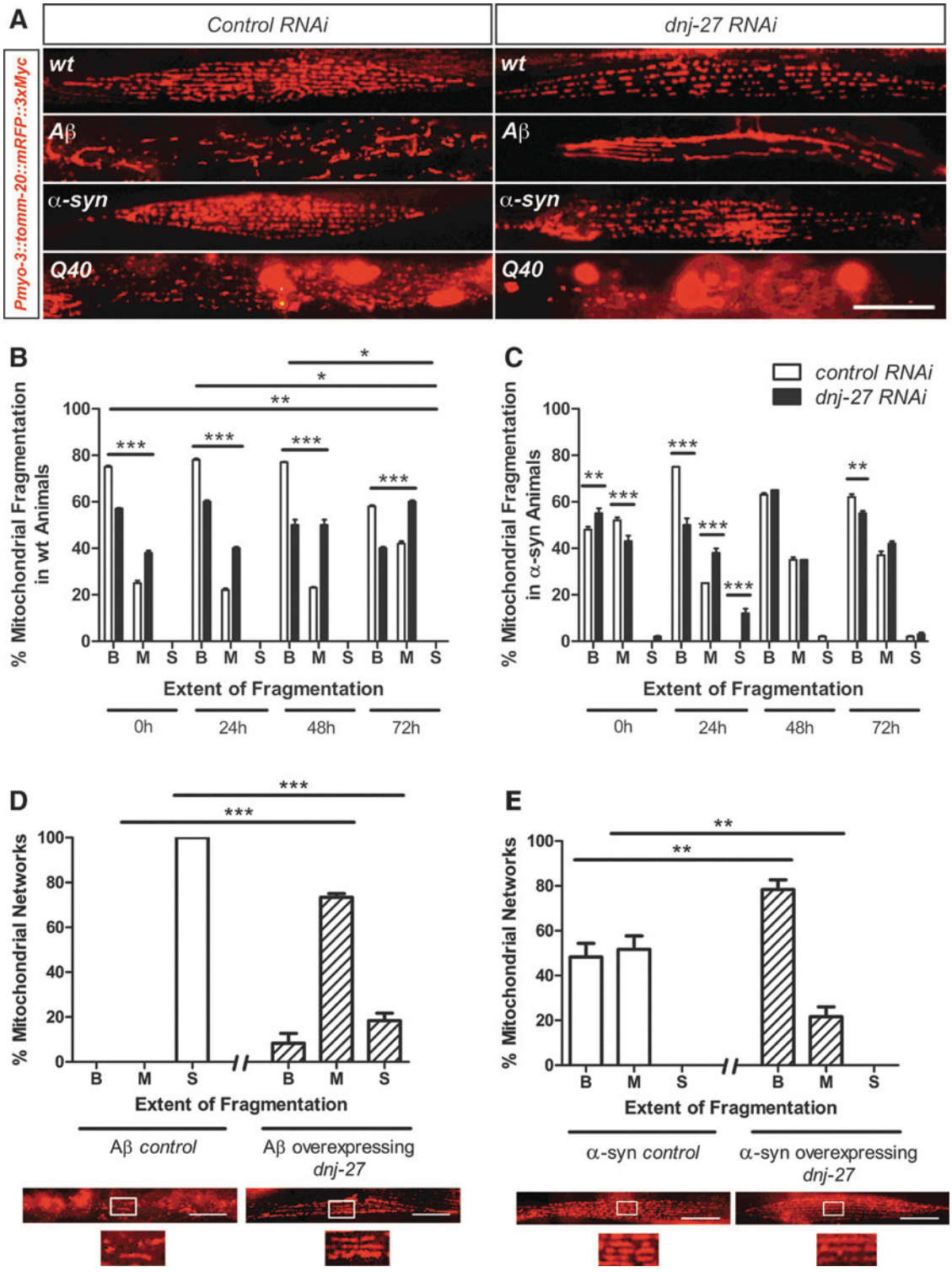

FIG. 7. Modulation of mitochondrial fragmentation phenotypes in Aβ, α-syn and Q40 worms by *dnj-27*. (A) Representative images of the mitochondrial fragmentation of worms expressing the *syEx1155 [Pmyo-3::tomm-20::mRFP]* reporter in A*β*, *α*-syn::YFP and Q40::YFP worms at the first day adulthood ($t = 0$ h) grown on HT115 bacteria expressing control and *dnj-27* RNAi constructs, respectively. Note the strong mitochondrial fragmentation in A*β* and Q40 worms grown in control RNAi bacteria that precluded any possible quantification of the enhancement of the phenotype upon *dnj-27* downregulation. **(B, C)** Quantification of the progressive mitochondrial fragmentation of wt and *α*-syn worms expressing the *syEx1155 [Pmyo-3::tomm-20::mRFP]* reporter grown on control or *dnj-27* RNAi bacteria. Experiments were completed with $n = 60$ animals per strain (mean ± SEM). Data were analyzed using a mixed model ANOVA which identifies a significant increase in the extent of fragmentation with time (***$p < 0.001$; **$p < 0.01$ and *$p < 0.05$). **(D, E)** Quantification of the improvement of the mitochondrial fragmentation of A*β* and *α*-syn worms expressing the *syEx1155 [Pmyo-3::tomm-20::mRFP]* reporter upon overexpression of DNJ-27. Worms were grown on HT115 bacteria for comparison with experiments in (A, C). Experiments were completed with $n = 60$ animals per strain (mean ± SEM). Data were analyzed using one-way ANOVA with a Bonferroni correction for multiple comparisons (**$p < 0.01$; ***$p < 0.001$). To see this illustration in color, the reader is referred to the web version of this article at www.liebertpub.com/ars

protein degradation *via* autophagy and proteasome pathways. A plausible explanation is that *dnj-27* inhibition compromises ERAD [as it has been previously shown for *ERdj5* inhibition in mammals (80)] leading to an alteration of ER homeostasis that, in turn, would result in an increase of the load of misfolded proteins retrotranslocated into the cytosol for degradation. Ultimately, the cells of a healthy animal would try to reduce this extra cargo of misfolded proteins in the cytoplasm by increasing their degradation. However, in the context of the ND models used in this work, it has been demonstrated that the accumulation of Aβ, α-syn, and polyQ causes an impairment of the proteasome and autophagy function (4, 16, 34, 51). Thus, the altered cytoplasmic proteostasis caused by *dnj-27* downregulation in these ND models cannot be relieved by these clearing mechanisms, hence resulting in a more sustained alteration of protein homeostasis and a net increase of misfolded proteins in the cytoplasm. As Gidalevitz *et al.* have elegantly shown (22), this disturbance of cytoplasmic proteostasis would favor the rapid aggregation of any aggregation-prone proteins, therefore explaining the effect on Aβ, α-syn and Q40 worms found upon *dnj-27* downregulation.

Supporting our hypothesis, similar results were obtained when other genes involved in ERAD and UPR were assayed. RNAi downregulation of *ire-1*, *xbp-1*, *pek-1*, *sel-1*, and *hrdl-1* resulted in increased cytosolic protein degradation. Nevertheless, knockdown of *atf-6*, *cup-2*, *R151.,6* and *sel-11/hrd-1* did not affect protein degradation. This could be explained by partially redundant gene function, as has been previously described for *cup-2* and *R151.6* in *C. elegans* (59). It is important to point out that, with the exception of *R151.6*, the protection observed with these genes was not extended to all the three ND models. This implies putative different mechanisms (from that proposed for *dnj-27)* for the impact of *cup-2*, *R151.6* and *sel-11/hrd-1* on polyQ and/or α-syn aggregation and on Aβ-dependent paralysis. Previous studies have related several aspects of the ERAD pathway to Aβ, α-syn or polyQ toxicity (10, 13, 33). For instance, α-syn has been found to inhibit ER-Golgi trafficking in yeast, resulting in the accumulation of specific misfolded proteins to be degraded by ERAD (10). Moreover, it has been demonstrated that entrapment of some essential ERAD proteins by polyQ-expanded huntingtin is an early event of toxicity in yeast and mammalian cells (13). Therefore, it is conceivable that different mechanisms may contribute to the cellular consequences observed in these *C. elegans* ND models and that other ERAD genes might then affect toxicity by distinct mechanisms.

Cytoplasmic aggregation of Aβ, α-syn, or polyQ in *C. elegans* has been linked to the pathological phenotypes associated to these peptides (25, 41, 58). The protective role of the *dnj-27* gene in paralysis and mobility tests certainly appears to correlate well with the level of aggregation of the specific toxic peptide in most cases, although a 100% correlation was not found. This is the case for α-syn worms treated with *dnj-27* RNAi and Q40 animals overexpressing *dnj-27*, where a mild (although statistically significant) increase or decrease in aggregation, respectively, did not result in any changes in toxicity. The most plausible explanation for the lack of correlation in these two specific cases is that an upper/lower aggregation threshold must be reached to induce the cellular and behavioral symptoms we measure in our studies.

In this context, whether aggregates are causal in ND progression remains controversial, as aggregates and inclusions have been linked both to toxicity and protection (2, 47, 56, 77). A recent study suggests that each aggregation-suppressor gene will have differential effects on toxicity depending on the affected cellular function and on its own network of interacting partners (63). For *dnj-27*, this appears to be the case since there is a strong correlation between ND proteins aggregation and toxicity, but other mechanisms underlying *dnj-27* protection cannot be ruled out. Key events in most ND include oxidative stress and mitochondrial dysfunction, among others (12, 21, 54, 68). In this study, we have confirmed the previously reported mitochondrial network disruption in Aβ and α-syn worms (17, 23, 32) and demonstrated for the first time that this is also the case for Q40 animals. We have found mitochondrial fragmentation upon *dnj-27* downregulation, thus suggesting that mitochondrial dynamics represents another potential factor implicated in *dnj-27* protection. Given the fact that the ER and the mitochondria are physically connected through MAMs (83), it is conceivable that disruption of ER function caused by *dnj-27* downregulation could negatively affect mitochondrial function. Indeed, *dnj-27* downregulation worsens the mitochondrial fragmentation of α-syn worms, while overexpression of DNJ-27 alleviates the mitochondrial fragmentation of Aβ and α-syn animals, supporting the notion that *dnj-27* might exert its protective function, at least in part, by regulating mitochondrial function.

Another important issue that has emerged from this study is the influence of the type of food source on the toxicity and aggregation phenotypes of the ND worm models. In this context, it has been shown that differences in food sources can have a profound effect on *C. elegans* lifespan and other parameters (45, 55). These differences can be explained by differing nutritional values of both HT115 and OP50 *E. coli* strains, since metabolic profiles and fat storage levels are not the same in worms grown on each bacteria (45, 55). Central to these issues is the insulin pathway, since it is known to mediate a large part of the sensory inputs on lifespan (1, 45) and to modulate pathogen resistance to bacteria (20). Importantly, toxicity in *C. elegans* ND models is influenced by the insulin pathway [(8, 9, 16, 47) and our own unpublished observations] providing a link between food source and proteotoxicity. Although the differences between the nematode and human diet are obvious, our observation is consistent with an increasing number of studies that support a role of environmental factors, such as diet and environmental toxins, in ND (52, 53, 73).

In conclusion, we have identified DNJ-27/ERdj5 as a novel regulator of age-related proteotoxicity in transgenic *C. elegans* models of ND. Different subcellular compartments appears to mediate the DNJ-27 protection since mitochondrial dynamics and cytoplasmic proteostasis disturbances, mechanisms previously identified in ND progression, are involved.

Materials and Methods

C. elegans *strains and culture conditions*

The standard methods for culturing and maintenance of *C. elegans* were used as described previously (69). The strains used in this work are described in Supplementary Table S1.

All experiments were performed at 20°C unless otherwise noted.

To induce ER stress, L4 worms were placed onto seeded nematode growth medium (NGM) plates containing 10, 20 and 30 μg/ml of tunicamycin (Sigma). One day adult animals were analyzed after 16 h of tunicamycin treatment.

RNA interference

HT115 *E. coli* strain transformed with either pL4440 empty vector or the respective RNAi test clones were grown in liquid Luria-Bertani medium containing 100 μg/ml ampicillin for 15 h at 37°C prior seeding the RNAi plates containing 1 m*M* isopropyl β-D-1-thiogalactopyranoside. The plates were incubated 2 days at 37°C to induce dsRNA. Phenotypes were scored in synchronized animals grown for two generations in the corresponding RNAi generated by allowing RNAi-treated gravid hermaphrodites to lay eggs during 2 h on fresh RNAi plates.

Plasmid constructs and transgenesis

All plasmid constructs used to generate the transgenic strains described in this work (see Supplementary Table S1) were made using the vector *pPD95.77* as backbone (Fire Vector Kit), with the following exceptions: *pVZ378* used a modified version of *pPD95.85* containing an ER signal peptide and a KDEL retention signal as described (37); *pVZ451* was constructed using a modified *pDEST* vector backbone (from the Gateway Cloning System; Invitrogen). *pVZ448* was generated using the *Pges-1::mCherry::TRAM-1* construct as described (75). The *Punc-122::GFP* and *Pmyo-2::mCherry* reporters were kind gifts from Piali Sengupta and Peter Askjaer, respectively. The *Ptrx-3::mCherry* reporter was generated in our lab (unpublished data). Information on baits, primers, cloning sites, sizes, and sequences of the different inserts as well as the amount of DNA injected for the constructs used to generate the corresponding transgenic strains will be provided upon request. Germline transformation was performed as described (46).

Microscopy

Animals were mounted in a 5 μl drop of 10 m*M* levamisole (Sigma) on a 3% agarose pad covered with a 24×24 mm coverslip. Differential interference contrast and fluorescence imaging was performed on a Zeiss AxioImager M2 ApoTome fluorescence microscope equipped with an AxioCam MRn. Images were captured with the AxioVision 4.8 Software (Zeiss). Confocal images were obtained with Leica AOBS SP2 and equal adjustment of brightness and contrast on control and matched experimental images was done using Adobe Photoshop 10 Software (Adobe Systems) and ImageJ (NIH).

Paralysis phenotype and β-amyloid deposit quantification

Synchronous populations of Aβ worms were generated by time-limited (2–3 h) egg lay at 16°C. Parents were then removed, and the progeny were grown continuously at 20°C. Paralysis scoring was initiated at the first day of adulthood and determined daily, whereby paralyzed worms were removed from plates. A worm was scored as paralyzed if it did not respond to a gentle touch stimulus with a platinum wire. In experiments measuring the paralysis of transgenic strains carrying extrachromosomal arrays, worms containing the transgene were identified by the fluorescence of the reporter included in the extrachromosomal array.

For amyloid deposit staining, worms were stained with the amyloid-specific dye X-34 (a kind gift from Prof. William Klunk) as previously described (42). Briefly, worms were propagated at 20°C and first-day adults were incubated for 2 h in 20 μl drops of 1 m*M* X-34 in 10 m*M* TRIS pH 7.5. Worms were then destained by rinsing once in a drop of phosphate buffered saline and then transferring them to NGM plates seeded with *E. coli* strain OP50 for overnight recovery at 20°C. Stained worms were anaesthetized with sodium azide and imaged with a Zeiss Axiophot epifluorescence microscope.

Impaired mobility phenotype quantification

Synchronous populations of α-syn or Q40 worms were generated by time-limited (2–3 h) egg lay at 20°C. Parents were removed, and progeny were grown continuously at 20°C. Impaired mobility scoring was initiated at the first day of adulthood and determined daily, whereby worms with compromised mobility were removed from plates. A worm was scored as mobility impaired if it did not move or was barely able to move a few millimeters after a gentle touch stimulus with a platinum wire. In experiments measuring the mobility of transgenic strains carrying extrachromosomal arrays, worms containing the transgene were identified by the fluorescence of the reporter included in the extrachromosomal array.

Quantification of aggregates

The number of α-syn aggregates was determined from the tip of the nose to the end of the second pharyngeal bulb using a Zeiss AxioImager M2 ApoTome fluorescence microscope equipped with an AxioCam MRn and ImageJ software for image analysis. Ten animals at day 1 of adulthood were included for each condition and each independent experiment.

The number of polyQ aggregates present in whole animals were counted at 40× magnification using a Zeiss AxioImager M2 ApoTome fluorescence microscope equipped with an AxioCam MRn. Twenty animals at day 1 of adulthood were included for each condition and each independent experiment.

Analysis of DA neurodegeneration

Worms were synchronized by time-limited (2–3 h) egg lay on NGM plates seeded with OP50 *E. coli* at 20°C. Progeny were transferred to a fresh plate containing 40 μg/ml 5-Fluoro-2′-deoxyuridine, to prevent eggs from hatching, when they reached late L4 stage. For each independent experiment, thirty 7-days old worms of each strain were examined under a Nikon Eclipse E800 epifluorescence microscope equipped with an Endow GFP HYQ filter cube (Chroma). The six anterior DA neurons (four CEP and two ADE DA neurons) were scored for neurodegeneration according to previously described criteria (3, 7).

Preparation of worm protein extracts and western blotting

For protein extraction, 100 worms from each strain (grown for two generations on the corresponding RNAi

bacteria or grown on OP50 for one generation) were manually collected at their first day of adulthood in 15 μl of Laemmli buffer. After freezing in liquid nitrogen, the mix was heated at 95°C for 10 min. For all immunoblots, proteins were separated by sodium dodecyl sulphate-polyacrylamide gel electrophoresis and transferred to Immobilon-P polyvinylidene fluoride membranes (Millipore). For Aβ, a 4–20% gradient polyacrylamide gel (BioRad) was used and blots were probed with anti-Aβ monoclonal 6E10 (Covance) at a 1:1000 dilution and mouse anti-immunoglobulin G (IgG; Sigma) at 1:10,000 as secondary antibody. For DNJ-27 detection (Supplementary Fig. S3A, B), a 1:500 dilution of rabbit anti-DNJ-27 primary antibody and a 1:10,000 dilution of horseradish peroxidase-conjugated goat anti-rabbit IgG secondary antibody (Sigma) were used. For α-syn::YFP and Q40::YFP detection, blots were probed with rabbit anti-GFP antibody (Santa Cruz) at a 1:500 dilution and a 1:10,000 dilution of the anti-rabbit as secondary antibody. The ECL kit (GE) was used for signal detection, following manufacturer's instructions. Monoclonal anti-α-tubulin (Sigma) 1:10,000 was used as loading control.

Analysis of muscle protein degradation, sarcomere structure, and mitochondrial network structure

Worms containing different transgenic reporters were used to assess potential subcellular defects in muscle (Supplementary Table S1). We used the same protocol as previously utilized for an analysis of known *C. elegans* muscle mutants (62); [for detailed consideration of the RNAi approach utilized see ref. (39)]. We employed two modifications to this past approach: (i) The effect of acute RNAi against a gene in a fully developed adult was assessed even if chronic growth on RNAi produced no subcellular defects; (ii) *ced-3*(*n717*) was used to assess if observed protein degradation required the protease CED-3. Briefly, animals were grown on RNAi for two generations. Subcellular phenotypes were recorded for 20–30 animals at the first day of adulthood and 24 h later in both the F1 and F2 generations (data not shown). Next, animals were age synchronized and grown to adulthood at which point the presence of normal cytosolic reporter protein, sarcomere structure, or mitochondrial network structure was confirmed [as previously described (62)], and then 100 adults, per condition, were placed on fresh plates containing RNAi against the gene of interest or control RNAi. Twenty-four hours later the presence of cytosolic reporter protein was assessed in 20–30 animals (not shown). At 48 (not shown) and 72 h post introduction to RNAi, the presence of cytosolic reporter protein, normal sarcomere structure, or normal mitochondrial network structure was assessed. For each individual time point, an RNAi treatment was scored as giving a subcellular defect in an individual animal if: (i) For cytosolic protein degradation: there was a visual loss of at least 30% of LacZ stain (*e.g.*, the worms looked light blue or "washed out" rather than dark blue); (ii) For sarcomere structure: there were at least two disorganized arrays of sarcomeres or at least two breaks in the normal array of sarcomeres in at least two muscle cells; (iii) For mitochondrial networks: at least a 25% lack of networked mitochondria in at least two muscle cells. For each individual time point, at least 20% of animals (above any baseline defects in the control RNAi animals) had to have been scored as having a defect for an overall defect to have been scored for the population.

Quantification of extent of fragmentation of mitochondrial networks within muscle

Pmyo-3::tomm-20::mRFP animals were grown on *control* RNAi (HT115) or *dnj-27* RNAi for two generations at 16°C before age synchronizing as previously described (90) then transferring L1's to 20°C for 72h (early adulthood, $t = 0$ h of experiment). Animals which expressed all the necessary transgenes were picked and imaged using a Zeiss AX10 microscope with an Axiocam MRC Digital camera and Axiovision LE software (Nottingham). Mitochondrial fragmentation was quantified in a three tier scoring system: "Baseline" which represented typical *wt* mitochondria expressing TOMM-20::mRFP (NB this baseline would be considered minor fragmentation in strain CB5600 which was used for the initial experiments in Figure 6); "Moderate fragmentation" which represented multiple obvious gaps in the networks of mitochondria; and "Severe fragmentation" which represented networks which were difficult to reconcile as mitochondria. Scoring was completed for $n = 20$ animals every 24 h from $t = 0$ h to $t = 72$ h inclusive and each experiment was completed in triplicate. In the *dnj-27* overexpression experiments roughly 20 adult animals which over expressed DNJ-27 and which were grown at 16°C, were picked to a fresh plate at 20°C, they were allowed to lay eggs for 24 h, and were then removed. At young adulthood, (roughly 96 h later) $n = 20$ animals which expressed all relevant transgenes were picked and scored. All DNJ-27 overexpression experiments were completed in triplicate. Image analysis and figure preparation was done with the GNU Image Manipulation Program. Scale bars represent 20 μm.

Statistical analysis

Microsoft Excel two-tail Student's *t*-test was used to calculate *p*-values in neurodegeneration assays and in Aβ deposits and aggregates quantification assays. A two-way analysis of variance was used to determine significance in the paralysis and mobility assays.

Acknowledgments

We thank the Caenorhabditis Genetics Center for providing worm strains and Drs. Piali Sengupta, Ellen Nollen, Xiaochen Wang, Peter Aksjaer, Richard Morimoto, Alexander Van der Bliek, Andrew Fire, Paul Sternberg, Amir Sapir and William Klunk for strains, constructs, and reagents. Continuous support from Peter Askjaer's and Manuel Muñoz's groups is deeply acknowledged. Drs. Laura Berkowitz, Adam J. Harrington and Alexander J. Burdette are gratefully acknowledged for excellent technical support and fruitful discussions. A.M.-V. was supported by the Instituto de Salud Carlos III (Projects PI080557 and PI1100072, cofinanced by the Fondo Social Europeo [FEDER]), Junta de Andalucía (Projects P07-CVI-02697 and P08-CVI-03629) and CSIC (Project PIE 200920I118). F.S. and N.J.S. were supported by NIH (AR-05342).

Author Disclosure Statement

No competing financial interests exist.

References

1. Apfeld J and Kenyon C. Regulation of lifespan by sensory perception in *Caenorhabditis elegans*. *Nature* 402: 804–809, 1999.
2. Arrasate M, Mitra S, Schweitzer ES, Segal MR, and Finkbeiner S. Inclusion body formation reduces levels of mutant huntingtin and the risk of neuronal death. *Nature* 431: 805–810, 2004.
3. Berkowitz LA, Hamamichi S, Knight AL, Harrington AJ, Caldwell GA, and Caldwell KA. Application of a *C. elegans* dopamine neuron degeneration assay for the validation of potential Parkinson's disease genes. *J Vis Exp* Pii: 835, 2008.
4. Boyd-Kimball D, Poon HF, Lynn BC, Cai J, Pierce WM, Jr., Klein JB, Ferguson J, Link CD, and Butterfield DA. Proteomic identification of proteins specifically oxidized in *Caenorhabditis elegans* expressing human Abeta(1–42): implications for Alzheimer's disease. *Neurobiol Aging* 27: 1239–1249, 2006.
5. Buchberger A, Bukau B, and Sommer T. Protein quality control in the cytosol and the endoplasmic reticulum: brothers in arms. *Mol Cell* 40: 238–252, 2010.
6. Cacho-Valadez B, Munoz-Lobato F, Pedrajas JR, Cabello J, Fierro-Gonzalez JC, Navas P, Swoboda P, Link CD, and Miranda-Vizuete A. The characterization of the *Caenorhabditis elegans* mitochondrial thioredoxin system uncovers an unexpected protective role of thioredoxin reductase 2 in beta-amyloid peptide toxicity. *Antioxid Redox Signal* 16: 1384–1400, 2012.
7. Cao S, Gelwix CC, Caldwell KA, and Caldwell GA. Torsin-mediated protection from cellular stress in the dopaminergic neurons of *Caenorhabditis elegans*. *J Neurosci* 25: 3801–3812, 2005.
8. Cohen E, Bieschke J, Perciavalle RM, Kelly JW, and Dillin A. Opposing activities protect against age-onset proteotoxicity. *Science* 313: 1604–1610, 2006.
9. Cohen E, Du D, Joyce D, Kapernick EA, Volovik Y, Kelly JW, and Dillin A. Temporal requirements of insulin/IGF-1 signaling for proteotoxicity protection. *Aging Cell* 9: 126–134, 2010.
10. Cooper AA, Gitler AD, Cashikar A, Haynes CM, Hill KJ, Bhullar B, Liu K, Xu K, Strathearn KE, Liu F, Cao S, Caldwell KA, Caldwell GA, Marsischky G, Kolodner RD, Labaer J, Rochet JC, Bonini NM, and Lindquist S. Alpha-synuclein blocks ER-Golgi traffic and Rab1 rescues neuron loss in Parkinson's models. *Science* 313: 324–328, 2006.
11. Cunnea PM, Miranda-Vizuete A, Bertoli G, Simmen T, Damdimopoulos AE, Hermann S, Leinonen S, Huikko MP, Gustafsson JA, Sitia R, and Spyrou G. ERdj5, an endoplasmic reticulum (ER)-resident protein containing DnaJ and thioredoxin domains, is expressed in secretory cells or following ER stress. *J Biol Chem* 278: 1059–1066, 2003.
12. Drake J, Link CD, and Butterfield DA. Oxidative stress precedes fibrillar deposition of Alzheimer's disease amyloid beta-peptide (1–42) in a transgenic *Caenorhabditis elegans* model. *Neurobiol Aging* 24: 415–420, 2003.
13. Duennwald ML and Lindquist S. Impaired ERAD and ER stress are early and specific events in polyglutamine toxicity. *Genes Dev* 22: 3308–3319, 2008.
14. Estevez AO, Mueller CL, Morgan KL, Szewczyk NJ, Teece L, Miranda-Vizuete A, and Estevez M. Selenium induces cholinergic motor neuron degeneration in *Caenorhabditis elegans*. *Neurotoxicology* 33: 1021–1032, 2012.
15. Fire A, Xu S, Montgomery MK, Kostas SA, Driver SE, and Mello CC. Potent and specific genetic interference by double-stranded RNA in *Caenorhabditis elegans*. *Nature* 391: 806–811, 1998.
16. Florez-McClure ML, Hohsfield LA, Fonte G, Bealor MT, and Link CD. Decreased insulin-receptor signaling promotes the autophagic degradation of beta-amyloid peptide in *C. elegans*. *Autophagy* 3: 569–580, 2007.
17. Fonte V, Dostal V, Roberts CM, Gonzales P, Lacor P, Magrane J, Dingwell N, Fan EY, Silverman MA, Stein GH, and Link CD. A glycine zipper motif mediates the formation of toxic beta-amyloid oligomers *in vitro* and *in vivo*. *Mol Neurodegener* 6: 61, 2011.
18. Fonte V, Kapulkin V, Taft A, Fluet A, Friedman D, and Link CD. Interaction of intracellular beta amyloid peptide with chaperone proteins. *Proc Natl Acad Sci U S A* 99: 9439–9444, 2002.
19. Fostel JL, Benner Coste L, and Jacobson LA. Degradation of transgene-coded and endogenous proteins in the muscles of *Caenorhabditis elegans*. *Biochem Biophys Res Commun* 312: 173–177, 2003.
20. Garsin DA, Villanueva JM, Begun J, Kim DH, Sifri CD, Calderwood SB, Ruvkun G, and Ausubel FM. Long-lived *C. elegans* daf-2 mutants are resistant to bacterial pathogens. *Science* 300: 1921, 2003.
21. Gibson GE and Huang HM. Oxidative stress in Alzheimer's disease. *Neurobiol Aging* 26: 575–578, 2005.
22. Gidalevitz T, Ben-Zvi A, Ho KH, Brignull HR, and Morimoto RI. Progressive disruption of cellular protein folding in models of polyglutamine diseases. *Science* 311: 1471–1474, 2006.
23. Gonzales PK and Link CD. Mitochondrial fission protects *C. elegans* from amyloid-beta toxicity. 18th International *C. elegans* Meeting Poster 394B, 2011.
24. Hagiwara M, Maegawa K, Suzuki M, Ushioda R, Araki K, Matsumoto Y, Hoseki J, Nagata K, and Inaba K. Structural basis of an ERAD pathway mediated by the ER-resident protein disulfide reductase ERdj5. *Mol Cell* 41: 432–444, 2011.
25. Hamamichi S, Rivas RN, Knight AL, Cao S, Caldwell KA, and Caldwell GA. Hypothesis-based RNAi screening identifies neuroprotective genes in a Parkinson's disease model. *Proc Natl Acad Sci U S A* 105: 728–733, 2008.
26. Hampton RY, Gardner RG, and Rine J. Role of 26S proteasome and HRD genes in the degradation of 3-hydroxy-3-methylglutaryl-CoA reductase, an integral endoplasmic reticulum membrane protein. *Mol Biol Cell* 7: 2029–2044, 1996.
27. Hardy J and Selkoe DJ. The amyloid hypothesis of Alzheimer's disease: progress and problems on the road to therapeutics. *Science* 297: 353–356, 2002.
28. Harman D. Aging: overview. *Ann N Y Acad Sci* 928: 1–21, 2001.
29. Harrington AJ, Hamamichi S, Caldwell GA, and Caldwell KA. *C. elegans* as a model organism to investigate molecular pathways involved with Parkinson's disease. *Dev Dyn* 239: 1282–1295, 2010.
30. Hayashi T and Su TP. Sigma-1 receptor chaperones at the ER-mitochondrion interface regulate Ca(2+) signaling and cell survival. *Cell* 131: 596–610, 2007.
31. Hosoda A, Tokuda M, Akai R, Kohno K, and Iwawaki T. Positive contribution of ERdj5/JPDI to endoplasmic reticulum protein quality control in the salivary gland. *Biochem J* 425: 117–125, 2010.
32. Kamp F, Exner N, Lutz AK, Wender N, Hegermann J, Brunner B, Nuscher B, Bartels T, Giese A, Beyer K, Eimer S, Winklhofer KF, and Haass C. Inhibition of mitochondrial fusion by alpha-synuclein is rescued by PINK1, Parkin and DJ-1. *EMBO J* 29: 3571–3589, 2010.
33. Kaneko M, Koike H, Saito R, Kitamura Y, Okuma Y, and Nomura Y. Loss of HRD1-mediated protein degradation

causes amyloid precursor protein accumulation and amyloid-beta generation. *J Neurosci* 30: 3924–3932, 2010.
34. Khan LA, Bauer PO, Miyazaki H, Lindenberg KS, Landwehrmeyer BG, and Nukina N. Expanded polyglutamines impair synaptic transmission and ubiquitin-proteasome system in *Caenorhabditis elegans*. *J Neurochem* 98: 576–587, 2006.
35. Kirstein-Miles J and Morimoto RI. *Caenorhabditis elegans* as a model system to study intercompartmental proteostasis: Interrelation of mitochondrial function, longevity, and neurodegenerative diseases. *Dev Dyn* 239: 1529–1538, 2010.
36. Knittler MR, Dirks S, and Haas IG. Molecular chaperones involved in protein degradation in the endoplasmic reticulum: quantitative interaction of the heat shock cognate protein BiP with partially folded immunoglobulin light chains that are degraded in the endoplasmic reticulum. *Proc Natl Acad Sci U S A* 92: 1764–1768, 1995.
37. Labrousse AM, Zappaterra MD, Rube DA, and van der Bliek AM. *C. elegans* dynamin-related protein DRP-1 controls severing of the mitochondrial outer membrane. *Mol Cell* 4: 815–826, 1999.
38. Lehmann S, Shephard F, Jacobson LA, and Szewczyk NJ. Integrated control of protein degradation in muscle. *Worm* 1: 141–150, 2012.
39. Lehmann S, Shephard F, Jacobson LA, and Szewczyk NJ. Using multiple phenotype assays and epistasis testing to enhance the reliability of RNAi screening and identify regulators of muscle protein degradation. *Genes (Basel)* 3: 686–701, 2012.
40. Lewis MJ and Pelham HR. A human homologue of the yeast HDEL receptor. *Nature* 348: 162–163, 1990.
41. Link CD. Expression of human beta-amyloid peptide in transgenic *Caenorhabditis elegans*. *Proc Natl Acad Sci U S A* 92: 9368–9372, 1995.
42. Link CD, Johnson CJ, Fonte V, Paupard M, Hall DH, Styren S, Mathis CA, and Klunk WE. Visualization of fibrillar amyloid deposits in living, transgenic *Caenorhabditis elegans* animals using the sensitive amyloid dye, X-34. *Neurobiol Aging* 22: 217–226, 2001.
43. Link CD, Taft A, Kapulkin V, Duke K, Kim S, Fei Q, Wood DE, and Sahagan BG. Gene expression analysis in a transgenic *Caenorhabditis elegans* Alzheimer's disease model. *Neurobiol Aging* 24: 397–413, 2003.
44. Ma Y and Hendershot LM. The unfolding tale of the unfolded protein response. *Cell* 107: 827–830, 2001.
45. Maier W, Adilov B, Regenass M, and Alcedo J. A neuromedin U receptor acts with the sensory system to modulate food type-dependent effects on *C. elegans* lifespan. *PLoS Biol* 8: e1000376, 2010.
46. Mello CC, Kramer JM, Stinchcomb D, and Ambros V. Efficient gene transfer in *C. elegans*: extrachromosomal maintenance and integration of transforming sequences. *EMBO J* 10: 3959–3970, 1991.
47. Morley JF, Brignull HR, Weyers JJ, and Morimoto RI. The threshold for polyglutamine-expansion protein aggregation and cellular toxicity is dynamic and influenced by aging in *Caenorhabditis elegans*. *Proc Natl Acad Sci U S A* 99: 10417–10422, 2002.
48. Mouysset J, Kahler C, and Hoppe T. A conserved role of *Caenorhabditis elegans* CDC-48 in ER-associated protein degradation. *J Struct Biol* 156: 41–49, 2006.
49. Nollen EA, Garcia SM, van Haaften G, Kim S, Chavez A, Morimoto RI, and Plasterk RH. Genome-wide RNA interference screen identifies previously undescribed regulators of polyglutamine aggregation. *Proc Natl Acad Sci U S A* 101: 6403–6408, 2004.
50. Orr HT and Zoghbi HY. Trinucleotide repeat disorders. *Annu Rev Neurosci* 30: 575–621, 2007.
51. Pivtoraiko VN, Harrington AJ, Mader BJ, Luker AM, Caldwell GA, Caldwell KA, Roth KA, and Shacka JJ. Low-dose bafilomycin attenuates neuronal cell death associated with autophagy-lysosome pathway dysfunction. *J Neurochem* 114: 1193–1204, 2010.
52. Priyadarshi A, Khuder SA, Schaub EA, and Priyadarshi SS. Environmental risk factors and Parkinson's disease: a metaanalysis. *Environ Res* 86: 122–127, 2001.
53. Ramesh BN, Rao TS, Prakasam A, Sambamurti K, and Rao KS. Neuronutrition and Alzheimer's disease. *J Alzheimers Dis* 19: 1123–1139, 2010.
54. Reddy PH and Reddy TP. Mitochondria as a therapeutic target for aging and neurodegenerative diseases. *Curr Alzheimer Res* 8: 393–409, 2011.
55. Reinke SN, Hu X, Sykes BD, and Lemire BD. *Caenorhabditis elegans* diet significantly affects metabolic profile, mitochondrial DNA levels, lifespan and brood size. *Mol Genet Metab* 100: 274–282, 2010.
56. Ross CA and Poirier MA. Protein aggregation and neurodegenerative disease. *Nat Med* 10 Suppl: S10–S17, 2004.
57. Sasagawa Y, Yamanaka K, and Ogura T. ER E3 ubiquitin ligase HRD-1 and its specific partner chaperone BiP play important roles in ERAD and developmental growth in *Caenorhabditis elegans*. *Genes Cells* 12: 1063–1073, 2007.
58. Satyal SH, Schmidt E, Kitagawa K, Sondheimer N, Lindquist S, Kramer JM, and Morimoto RI. Polyglutamine aggregates alter protein folding homeostasis in *Caenorhabditis elegans*. *Proc Natl Acad Sci U S A* 97: 5750–5755, 2000.
59. Schaheen B, Dang H, and Fares H. Derlin-dependent accumulation of integral membrane proteins at cell surfaces. *J Cell Sci* 122: 2228–2239, 2009.
60. Schekman R. Cell biology: a channel for protein waste. *Nature* 429: 817–818, 2004.
61. Shen X, Ellis RE, Lee K, Liu CY, Yang K, Solomon A, Yoshida H, Morimoto R, Kurnit DM, Mori K, and Kaufman RJ. Complementary signaling pathways regulate the unfolded protein response and are required for *C. elegans* development. *Cell* 107: 893–903, 2001.
62. Shephard F, Adenle AA, Jacobson LA, and Szewczyk NJ. Identification and functional clustering of genes regulating muscle protein degradation from amongst the known *C. elegans* muscle mutants. *PLoS One* 6: e24686, 2011.
63. Silva MC, Fox S, Beam M, Thakkar H, Amaral MD, and Morimoto RI. A genetic screening strategy identifies novel regulators of the proteostasis network. *PLoS Genet* 7: e1002438, 2011.
64. Simmen T, Aslan JE, Blagoveshchenskaya AD, Thomas L, Wan L, Xiang Y, Feliciangeli SF, Hung CH, Crump CM, and Thomas G. PACS-2 controls endoplasmic reticulum-mitochondria communication and Bid-mediated apoptosis. *EMBO J* 24: 717–729, 2005.
65. Simmer F, Tijsterman M, Parrish S, Koushika SP, Nonet ML, Fire A, Ahringer J, and Plasterk RH. Loss of the putative RNA-directed RNA polymerase RRF-3 makes *C. elegans* hypersensitive to RNAi. *Curr Biol* 12: 1317–1319, 2002.
66. Singleton AB, Farrer M, Johnson J, Singleton A, Hague S, Kachergus J, Hulihan M, Peuralinna T, Dutra A, Nussbaum R, Lincoln S, Crawley A, Hanson M, Maraganore D, Adler C, Cookson MR, Muenter M, Baptista M, Miller D, Blancato J, Hardy J, and Gwinn-Hardy K. alpha-Synuclein locus triplication causes Parkinson's disease. *Science* 302: 841, 2003.

67. Spillantini MG, Crowther RA, Jakes R, Hasegawa M, and Goedert M. alpha-Synuclein in filamentous inclusions of Lewy bodies from Parkinson's disease and dementia with lewy bodies. *Proc Natl Acad Sci U S A* 95: 6469–6473, 1998.
68. Su B, Wang X, Zheng L, Perry G, Smith MA, and Zhu X. Abnormal mitochondrial dynamics and neurodegenerative diseases. *Biochim Biophys Acta* 1802: 135–142, 2010.
69. Sulston J and Hodgkin J. Methods. In: *The Nematode Caenorhabditis elegans*. edited by Press CSHL. New York: Cold Spring Harbor, 1988, pp. 587–606.
70. Szabadkai G, Bianchi K, Varnai P, De Stefani D, Wieckowski MR, Cavagna D, Nagy AI, Balla T, and Rizzuto R. Chaperone-mediated coupling of endoplasmic reticulum and mitochondrial Ca2+ channels. *J Cell Biol* 175: 901–911, 2006.
71. Szewczyk NJ, Peterson BK, Barmada SJ, Parkinson LP, and Jacobson LA. Opposed growth factor signals control protein degradation in muscles of *Caenorhabditis elegans*. *EMBO J* 26: 935–943, 2007.
72. Szewczyk NJ, Peterson BK, and Jacobson LA. Activation of Ras and the mitogen-activated protein kinase pathway promotes protein degradation in muscle cells of *Caenorhabditis elegans*. *Mol Cell Biol* 22: 4181–4188, 2002.
73. Tanner CM. Is the cause of Parkinson's disease environmental or hereditary? Evidence from twin studies. *Adv Neurol* 91: 133–142, 2003.
74. Taylor JP, Hardy J, and Fischbeck KH. Toxic proteins in neurodegenerative disease. *Science* 296: 1991–1995, 2002.
75. Tian Y, Li Z, Hu W, Ren H, Tian E, Zhao Y, Lu Q, Huang X, Yang P, Li X, Wang X, Kovacs AL, Yu L, and Zhang H. *C. elegans* screen identifies autophagy genes specific to multicellular organisms. *Cell* 141: 1042–1055, 2010.
76. Travers KJ, Patil CK, Wodicka L, Lockhart DJ, Weissman JS, and Walter P. Functional and genomic analyses reveal an essential coordination between the unfolded protein response and ER-associated degradation. *Cell* 101: 249–258, 2000.
77. Treusch S, Cyr DM, and Lindquist S. Amyloid deposits: protection against toxic protein species? *Cell Cycle* 8: 1668–1674, 2009.
78. Uehara T, Nakamura T, Yao D, Shi ZQ, Gu Z, Ma Y, Masliah E, Nomura Y, and Lipton SA. S-nitrosylated protein-disulphide isomerase links protein misfolding to neurodegeneration. *Nature* 441: 513–517, 2006.
79. Urano F, Calfon M, Yoneda T, Yun C, Kiraly M, Clark SG, and Ron D. A survival pathway for *Caenorhabditis elegans* with a blocked unfolded protein response. *J Cell Biol* 158: 639–646, 2002.
80. Ushioda R, Hoseki J, Araki K, Jansen G, Thomas DY, and Nagata K. ERdj5 is required as a disulfide reductase for degradation of misfolded proteins in the ER. *Science* 321: 569–572, 2008.
81. van Ham TJ, Holmberg MA, van der Goot AT, Teuling E, Garcia-Arencibia M, Kim HE, Du D, Thijssen KL, Wiersma M, Burggraaff R, van Bergeijk P, van Rheenen J, Jerre van Veluw G, Hofstra RM, Rubinsztein DC, and Nollen EA. Identification of MOAG-4/SERF as a regulator of age-related proteotoxicity. *Cell* 142: 601–612, 2010.
82. van Ham TJ, Thijssen KL, Breitling R, Hofstra RM, Plasterk RH, and Nollen EA. *C. elegans* model identifies genetic modifiers of alpha-synuclein inclusion formation during aging. *PLoS Genet* 4: e1000027, 2008.
83. Vance JE. Phospholipid synthesis in a membrane fraction associated with mitochondria. *J Biol Chem* 265: 7248–7256, 1990.
84. Vembar SS and Brodsky JL. One step at a time: endoplasmic reticulum-associated degradation. *Nat Rev Mol Cell Biol* 9: 944–957, 2008.
85. Voisine C, Pedersen JS, and Morimoto RI. Chaperone networks: tipping the balance in protein folding diseases. *Neurobiol Dis* 40: 12–20, 2010.
86. Wang H, Lim PJ, Karbowski M, and Monteiro MJ. Effects of overexpression of huntingtin proteins on mitochondrial integrity. *Hum Mol Genet* 18: 737–752, 2009.
87. Yamanaka K, Okubo Y, Suzaki T, and Ogura T. Analysis of the two p97/VCP/Cdc48p proteins of *Caenorhabditis elegans* and their suppression of polyglutamine-induced protein aggregation. *J Struct Biol* 146: 242–250, 2004.
88. Ye Y, Shibata Y, Yun C, Ron D, and Rapoport TA. A membrane protein complex mediates retro-translocation from the ER lumen into the cytosol. *Nature* 429: 841–847, 2004.
89. Yoshida H, Matsui T, Hosokawa N, Kaufman RJ, Nagata K, and Mori K. A time-dependent phase shift in the mammalian unfolded protein response. *Dev Cell* 4: 265–271, 2003.
90. Zdinak LA, Greenberg IB, Szewczyk NJ, Barmada SJ, Cardamone-Rayner M, Hartman JJ, and Jacobson LA. Transgene-coded chimeric proteins as reporters of intracellular proteolysis: starvation-induced catabolism of a lacZ fusion protein in muscle cells of *Caenorhabditis elegans*. *J Cell Biochem* 67: 143–153, 1997.

Address correspondence to:
Dr. Antonio Miranda-Vizuete
Instituto de Biomedicina de Sevilla (IBIS)
Hospital Universitario Virgen del Rocío/CSIC
Universidad de Sevilla
Laboratorio 118, Avd. Manuel Siurot s/n
Sevilla 41013
Spain

E-mail: amiranda-ibis@us.es

Date of first submission to ARS Central, October 30, 2012; date of final revised submission, April 28, 2013; date of acceptance, May 5, 2013.

Abbreviations Used

α-syn = alpha-synuclein
Aβ = beta amyloid peptide
AD = Alzheimer disease
ANOVA = analysis of variance
cDNA = complementary DNA
DA = dopaminergic
ER = endoplasmic reticulum
ERAD = ER-associated degradation
GFP = green fluorescent protein
HD = Huntington disease
IgG = immunoglobulin G
MAM = mitochondria-associated membrane
ND = neurodegenerative diseases
NGM = nematode growth medium
PD = Parkinson disease
polyQ = polyglutamine
RNAi = RNA interference
SEM = standard error of the mean
Trx = thioredoxin
UPR = unfolded protein response
UTR = untranslated region
YFP = yellow fluorescent protein